UNIVERSITY OF TROMSØ UIT

FACULTY OF SCIENCE AND TECHNOLOGY
DEPARTMENT OF PHYSICS AND TECHNOLOGY

Experimental and numerical estimation of ultrasonic attenuation in polymers based on wave transmission methods

Trude Ediassen Grimstad

FYS-3921 Master's Thesis in Electrical Engineering

July 2013

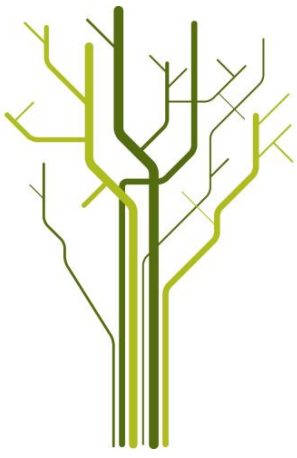

Acknowledgements

First of all I would like to thank my supervisor Frank Melandsø and my co-supervisor Svein Jacobsen for all their help during my work with this thesis. I want to thank the project "Subsea Sensors for Oil and Gas", for giving me this interesting topic. I would also like to thank Sanat Wagle and Adit Decharat for their help on the lab.

Abstract

PI-film, also known as Kapton, is a widely used polymer in the production of electronic equipment. Its use in printed circuit boards and sensors is increasing. It is therefore important to have knowledge about ultrasonic attenuation in the polymer.

The main goal of this thesis was to investigate the attenuation of ultrasound through different polymers with different thicknesses. The presentation is divided into two parts based on the polymer thickness with respect to the applied wavelength. The attenuation was examined through both experimental methods and numerical studies were this was possible. Basic theory of waves, elastic materials and attenuation in polymers are presented, and theoretical models were applied to compare the attenuation found through experiments and simulation.

Experimental investigation of thick polymer samples were done with two transducers operating best at 10- and 20 MHz, respectively. Corresponding total transmission coefficients and damping factors were obtained. Comparisons with theory suggests highest reliability for the results obtained with the 10 MHz transducers.

10 MHz transducers were applied in the experiments with thin Kapton-based samples. Based on the experiment, COMSOL Multiphysics was used to implement realistic models for numerical simulation. The amplitude spectra obtained through both experiments and simulations were compared to a corresponding theoretical spectrum. The model differences taken into consideration, the resulting amplitude spectra from the three methods were found to coincide. An experimental investigation at 10 MHz of the effects of surface treatment between layers in two PVDF-coated Kapton films were performed. At this frequency, no differences in transmission properties between the treated and untreated samples were detected.

Contents

Chapter 1

Introduction

1.1 History of the transducer

This history introduction is taken from the Project paper "Ultrasonic diffraction fields in fluids and elastic materials" [11], and has been written based on information found in the books "Principles of Sonar Performance Modelling" [1] by Michael Ainslie, "Diagnostic Ultrasound Imaging: Inside out" [30] by Thomas L. Szabo, and "Fundamentals and Applications of ultrasonic waves" [7] by J. David N. Cheeke.

Several discoveries lead up to the invention of sonar. In 1816, François Beudant measured the speed of sound in seawater by using an underwater bell and a swimmer waving a flag. For the same measurement setup, Colladon and Sturm build an improved light-sound synchronization system in 1826.

A very important contribution to the commence of transducers and ultrasound technology was made by the two brothers Pierre and Jacques Curie in 1880, when they discovered that the mechanical deformation of some crystals would create electrical charge (piezoelectricity). In 1881, they also confirmed the reversed piezoelectric effect, when they showed that some crystals would deform by applying voltage to them. This discovery, together with the invention of the triode amplifier tube by Lee De Forest in 1907, lead to further advances in pulse-echo range measurements.

The historical event that is considered most important for the coming of sonar and ultrasound, was the tragic sinking of RMS Titanic after having smashed into an undetected underwater iceberg in 1912. Scientists began to search for ways of detecting, and warn ships about underwater obstacles.

Figure 1.1: Robert Boyle. Image found on November 29, 2012 on the University of Alberta webpage: http://www.100years.ualberta.ca/ [23]

Already in 1913, Reginald Fessenden filed patents on an electromagnetic transducer. The year after he demonstrated its use by detecting an iceberg nearly two miles away. The device later became known as the Fessenden oscillator.

The extensive use of submarines during World War I lead French and British scientists into research to find methods of detecting underwater vessels in 1915. The French primarily worked on echolocation, or "active sonars" - while the British mostly worked with listening devices called hydrophones or "passive sonars". The active sonars consist of a sound transmitter and a receiver detecting echoes from the transmitted sound. The passive sonars use only a receiver, which was listening for sound that the target was emitting.

The same year a group of scientists formed The Board of Invention and Research (BIR) in Scotland, and by the year 1917 the group consisted of more than 80 people. Amongst them were the British physicist Albert Beaumond Wood and the Canadian physicist Robert Boyle, working on passive listening and echolocation. The first breakthrough came in 1917 when Boyle detected submarines at a distance of 910 meters with the Fessenden oscillator. However, the 1 kHz frequency of the Fessenden transmitter was too low to give the necessary resolution, and the work with this oscillator was abandoned. Also in 1917, Paul Langevin was working on the piezoelectric material quartz in France. Together with the invention of the valve amplifier by Brillouin and Beauvais, the quartz system "gave a signaling distance of up to six kilometers" by the end of 1917 (Hackmann, 1984, p.81 [12]). When French and British scientists started to work together in 1917, Boyle visited Langevin, and shortly after he too began to work on quartz transducers. In 1918, the same month as World War I ended, Boyle had built the first functional active sonar. At the time, the technology was known as "asdics", the term "sonar" was not used before in 1942. Figure 1.1 shows a portrait of

Boyle.

In 1915, portable omnidirectional hydrophones were available on the marked. In 1917, directional hydrophones also became available.

World War I set the stage for both passive and active sonars. While passive sonars underwent a gradual development that took centuries, active sonars were developed in a rush between 1915 and 1917. However, active sonars did not become available in time to be used in this war. Passive sonars on the other hand were used in this periode. In the peacetime following World War I, work began in order to determine safe conditions for the use of ultrasound in medicine. Sonar was used to measure water depth, and to locate fish. In 1922, a recording echo sounder was built by Marti and Langevin. The invention gave the possibility of preserving the output of the sounder in paper format.

In 1921, the Applied Research Laboratory (ARL) was founded. In 1928 they developed the magnetostrictive transducer. A magnetostrictive material converts magnetic energy to mechanical energy, and the other way around.

Another boost in the research of transducer technology was the result of investments of scientific resources for military purposes after the Japanese attack of Pearl Harbor during World War II, which caused USA to enter the war. USA obtained, during the war, an understanding of the propagation and scattering of sound in water. Also, a radar was created by applying pulse-echo ranging to electromagnetic waves.

In 1940, F. Firestone invented the Supersonic reflectoscope, which used the echo-range principle to locate defects in metal. This type of echo-ranging system uses a transmitter to excite a transducer. The transducer sends out series of repetitive ultrasonic pulses into a test object. Echoes from boundaries and different targets inside the test object were amplified and displayed as amplitude versus time on an oscilloscope. The display was known as “A-mode”, “A-line” or “A-scope”, where the “A” stands for amplitude. A-mode was the precursor to diagnostic ultrasound.

An important achievement for the use of ultrasound in medicine was the first through-transmission ultrasound attenuation image of the brain, witch marked the beginning of Echoencephalography. The image, created by the Dussik brothers in 1942, was made by storing the intensity output of a light bulb connected to the output of the receiving transducer.

Imaging methods were a topic of great interest in the 1950s. During this time, one of the first hand held contact scanners was build by Reid and Wild. To detect the transducer position in space, this imaging system used a position sensor that was triggered by periodically timed transmit pulses. To indicate depth, the echo output was shown on a display consisting of time traces that run from

the top to the bottom on the screen. The brightness of each time trace were proportional to the echo amplitude. This display became known as a "B-mode" or a "B-scan", where the "B" stands for brightness. The differences between the A-mode and B-mode display made it difficult to achieve consistent results.

The invention of digital computers and transistors in the late 1940 caused profound alterations in ultrasound imaging. Additional speed was added to the imaging development when Jack Kilby invented the integrating circuit in 1958, which consisted of multiple transistors and circuit elements. In 1971, one chip could carry 2300 transistors. Advancements in electronics caused the imaging quality to improve rapidly throughout the 1980's. In 1985, Robert Ballard and Jean Louis Michel discovered the wreck of RMS Titanic at a depth of 3800 meters by use of a submersible with side-scan sonar attached to it. Phased array design also evolved as a consequence of the developments in complementary technologies, and in the 1990's the bandwidth got wider and transducers could take matrix array configurations.

The advances in transducer technology and the field of ultrasonics has evolved rapidly the last 30 years.

1.2 Own contribution

In this thesis, ultrasonic transducers were used to investigate attenuation parameters in different polymers. A transducer was applied to transmit a broad banded signal through a polymer sample emerged into water. Another transducer was used to listen for the transmitted pulse on the opposite side of the polymer. The detected signals were displayed as voltage amplitude versus time, or A-mode, on an oscilloscope.

1.3 Project structure

Chapter 2 presents relevant theory for this thesis. Section 2.1 gives an introduction to elastic materials. 1-D wave theory is introduced in section 2.2. Theory for attenuation in thick and thin polymers is described in section 2.3 and 2.4.

The method applied to produce experimental and numerical results are given in chapter 3. The setup of the experiments are presented in section 3.1, next in section 3.2 the numerical models made in COMSOL Multiphysics are described. Finally, section 3.3 gives a short description of the signal analysis.

Chapter 4 displays the results. The results obtained through experiments are given in section 4.1. Next the results obtained by theoretical means and through simulations are presented in section 4.2. The final section in chapter 4 compares the results achieved through theory, simulations and experiments.

The results are discussed systematically in chapter 5, and a conclusion is given in chapter 6 together with suggestions for further work.

Chapter 2

Theory

2.1 Elastic materials

An elastic material can be deformed if exposed to some force F, and will return to its initial form when the force is removed. The following theory was written based on notes from Frank Melandsø [20], and the book "Elastic Waves in Solids I" [27], and is an extension of the same theory given in the Project paper "Ultrasonic diffraction fields in fluids and elastic materials' "[11].

2.1.1 Tensor notation

We start by defining the notation with general linear relations for tensors [20]:

1. **Scalar;** tensor of order 0. $\overline{u} = av$

2. **Vector;** tensor of order 1 $\overline{u}_i = \sum_{u=1}^{3} a_{i,k} v_k; \quad i = 1, 2, 3$

3. **Matrix;** tensor of order 2 $\overline{u}_{i,j} = \sum_{k=1}^{3} \sum_{l=1}^{3} a_{i,j,k,l} v_{k,l}; \quad i = 1, 2, 3, \ j = 1, 2, 3$

Tensors of higher order will be denoted in the same manner with its order represented by the number of elements.

2.1.2 Deformation

Figure 2.1 shows an elastic object in 1-D before and after it is being exposed to an external force F. Before the force is added, p_1 and p_2 are two points in the elastic medium positioned at x and $x + \Delta x$ on a reference line, respectively. After applying the force to both sides of the medium, the two points change positions to x' and $x' + \Delta x'$. The displacement u, of p_1 and p_2 is given by [27]:

$$u(x) = x' - x \tag{2.1}$$

$$u(x + \Delta x) = x' + \Delta x' - x - \Delta x = u(x) + \Delta x' - \Delta x = u(x) + \Delta u(x) \tag{2.2}$$

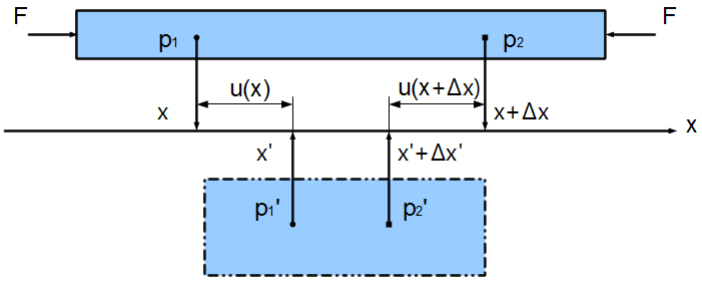

Figure 2.1: Deformation of a elastic material [27].

In 3-D, the positions of the two points p_1 and p_2 are described by the vectors $\underline{r}$ and $\underline{r} + \Delta\underline{r}$, respectively, as showed in Figure 2.2. The displacement $\underline{u}$ in this case is calculated by [20]:

$$\underline{u}(\underline{r}) = \underline{r}' - \underline{r} \tag{2.3}$$

$$\underline{u}(\underline{r} + \Delta\underline{r}) = \underline{r}' + \Delta\underline{r}' - \underline{r} - \Delta\underline{r} = \underline{u}(\underline{r}) + \Delta\underline{r}' - \Delta\underline{r} = \underline{u}(\underline{r}) + \Delta\underline{u}(\underline{r}) \tag{2.4}$$

which in component form becomes:

$$u_i(\underline{r} + \Delta\underline{r}) = u_i(\underline{r}) + \Delta u_i(\underline{r}) = u_i(\underline{r}) + \frac{\delta u_i}{\delta \underline{r}}\Delta\underline{r} \tag{2.5}$$

$$= u_i(\underline{r}) + \frac{\delta u_i}{\delta x}\Delta x + \frac{\delta u_i}{\delta y}\Delta y + \frac{\delta u_i}{\delta z}\Delta z, \quad i = 1, 2, 3 \tag{2.6}$$

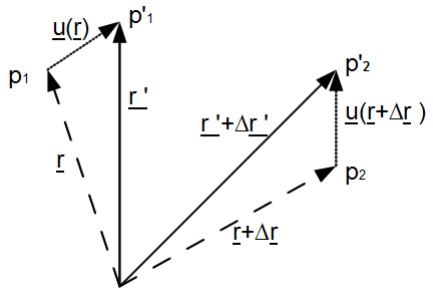

Figure 2.2: Deformation of an elastic material in three dimensions, [27] [20].

In vector notation, the displacement described above becomes:

$$\begin{bmatrix} u_x \\ u_y \\ u_z \end{bmatrix}_{\underline{r}+\Delta\underline{r}} = \begin{bmatrix} u_x \\ u_y \\ u_z \end{bmatrix} + \begin{bmatrix} \frac{\delta u_x}{\delta x} & \frac{\delta u_x}{\delta y} & \frac{\delta u_x}{\delta z} \\ \frac{\delta u_y}{\delta x} & \frac{\delta u_y}{\delta y} & \frac{\delta u_y}{\delta z} \\ \frac{\delta u_z}{\delta x} & \frac{\delta u_z}{\delta y} & \frac{\delta u_z}{\delta z} \end{bmatrix} \begin{bmatrix} \Delta x \\ \Delta y \\ \Delta z \end{bmatrix} = \underline{u}(\underline{r}) + \overline{J}_{ij}\Delta\underline{r} \tag{2.7}$$

where $\overline{J}_{ij}$ is the Jacobian matrix [8].

Strain

In 1-D the strain S is defined as the deformation per unit length. From equations (2.1) and (2.2) above we get that:

$$S = \lim_{\Delta x \to 0} \frac{\Delta u}{\Delta x} = \lim_{\Delta x \to 0} \frac{\Delta x' - \Delta x}{\Delta x} = \frac{\delta u}{\delta x} \tag{2.8}$$

In 3-D, the deformation assumed invariant to both translation and rotation, is defined as the symmetric part $\overline{S}_{ij}$, of the Jacobian matrix $\overline{J}_{ij}$ given in equation (2.7). The elements of the Jacobian matrix are:

$$\frac{\delta u_i}{\delta x_j} = \frac{1}{2}(\frac{\delta u_i}{\delta x_j} + \frac{\delta u_j}{\delta x_i}) + \frac{1}{2}(\frac{\delta u_i}{\delta x_j} - \frac{\delta u_j}{\delta x_i}) = \overline{S}_{ij} + \overline{\Omega}_{ij} \tag{2.9}$$

The strain is therefore defined as the second order tensor [27]:

$$\overline{S}_{ij} = \frac{1}{2}(\frac{\delta u_i}{\delta x_j} + \frac{\delta u_j}{\delta x_i}) \tag{2.10}$$

Stress

Consider a small cubic volume V, with surfaces $\Delta\varsigma_k$. On surface $\Delta\varsigma_3$ a small force $\Delta\underline{F}$ is acting, as shown in Figure 2.3. The force is given by:

$$\Delta\underline{F} = \Delta F_1\underline{e_1} + \Delta F_2\underline{e_2} + \Delta F_3\underline{e_3} \tag{2.11}$$

where e_1, e_2 and e_3 are the orthogonal basis vectors [15].

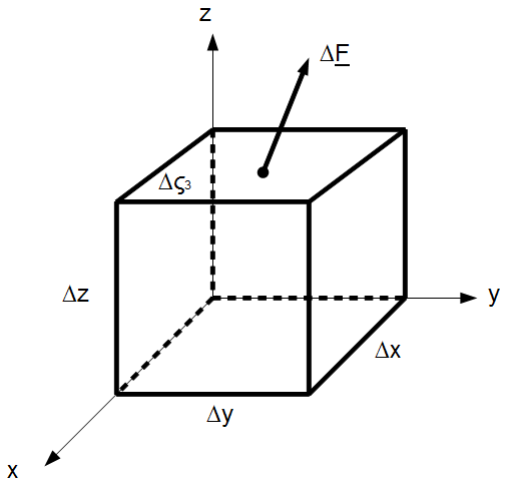

Figure 2.3: A cubic volume [20].

The force $\Delta\underline{F}$ produces the stress tensor $\overline{T}_{i3}$ on surface $\Delta\varsigma_3$, which can be described by:

$$\overline{T}_{i3} = \lim_{\Delta\varsigma_3 \to 0} \frac{\Delta F_i}{\Delta\varsigma_3} \tag{2.12}$$

The general expression for the second order stress tensor produced on the surfaces is [27]:

$$\overline{T}_{ik} = \lim_{\Delta\varsigma_k \to 0} \frac{\Delta F_i}{\Delta\varsigma_k} \tag{2.13}$$

2.1.3 Elastic constants

Young's modulus and Poisson's ratio

Young's modulus E and Poisson's ratio γ are quantities that can be determined experimentally.

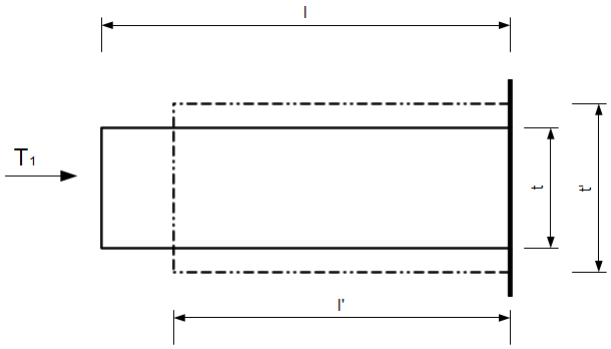

Figure 2.4: An elastic cylinder with radius t and length l [20].

Imagine an elastic cylinder with radius t and length l, as shown in Figure 2.4 . When imposing the stress T_1 to the top of the cylinder, the length shrinks into l' and the radius increases into t'. If these values are measured, the deformations (strains) S_1 and S_2 can be calculated by:

$$S_1 = \frac{l' - l}{l} \tag{2.14}$$

$$S_2 = \frac{t' - t}{t} \tag{2.15}$$

Then, from the calculated deformations and the value of imposed stress, Young's modulus can be determined by [20]:

$$E = \frac{T_1}{S_1} \tag{2.16}$$

And Poisson's ratio by:

$$\gamma = -\frac{S_2}{S_1} \tag{2.17}$$

Lamè coefficients

The Lamè constants λ and μ are related to Young's modulus E and Poisson's ratio γ by [27]:

$$\lambda = \frac{E\gamma}{(1+\gamma)(1-2\gamma)} \tag{2.18}$$

and

$$\mu = \frac{E}{2(1+\gamma)} \tag{2.19}$$

2.1.4 Hooke's law for elastic materials

Hooke's law in a elastic material can be described as a linear relation between the second order stress tensor $\overline{T}_{i,j}$ and the second order strain tensor $\overline{S}_{k,l}$ as [27]:

$$\overline{T}_{i,j} = \sum_k \sum_l \overline{c}_{i,j,k,l} \overline{S}_{k,l} \tag{2.20}$$

where $\overline{c}_{i,j,k,l}$ is a tensor of order 4.

Symmetry relations in a tensor

There are a maximum of $3^4 = 81$ elements in a 4-D tensor $\overline{c}_{i,j,k,l}$. Because of symmetries in the second order stress tensor $\overline{T}_{i,j}$ and in the second order strain tensor $\overline{S}_{k,l}$, only 36 of the elements are independent [20]. Thus,

$$\overline{T}_{i,j} = \overline{T}_{j,i} \Rightarrow \overline{c}_{i,j,k,l} = \overline{c}_{j,i,k,l} \tag{2.21}$$

$$\overline{S}_{k,l} = \overline{S}_{l,k} \Rightarrow \overline{c}_{i,j,k,l} = \overline{c}_{i,j,l,k} \tag{2.22}$$

Isotropic medium

An isotropic medium is a material that has uniform density along all directions. The tensor $\overline{c}_{i,j,k,l}$ of an isotropic material can be expressed by [27]:

$$\overline{c}_{i,j,k,l} = \lambda\ \overline{\delta}_{i,j}\overline{\delta}_{k,l} + \mu(\overline{\delta}_{i,k}\overline{\delta}_{j,l} - \overline{\delta}_{i,l}\overline{\delta}_{j,k}) \tag{2.23}$$

where λ and μ are the Lamè coefficients defined by the equations (2.18) and (2.19), respectively.

Dimension reduction

The 4-D tensor $\bar{c}_{i,j,k,l}$ can be transformed into a 2-D tensor with 6×6 elements. $\overline{S}_{k,l}$ and $\overline{T}_{i,j}$ must then be transformed into 6×1 vectors. These transformations are obtained by giving the index-couples (i, j), and equivalently (k, l), new names [20]:

$$(1,1) \rightarrow 1 \tag{2.24}$$
$$(2,2) \rightarrow 2 \tag{2.25}$$
$$(3,3) \rightarrow 3 \tag{2.26}$$
$$(2,3) = (3,2) \rightarrow 4 \tag{2.27}$$
$$(3,1) = (1,3) \rightarrow 5 \tag{2.28}$$
$$(1,2) = (2,1) \rightarrow 6 \tag{2.29}$$

Using this notation, Hooke's law from equation (2.20) can be written as $\overline{T}_i = \bar{c}_{ij}\overline{S}_i$, that is:

$$\begin{bmatrix} T_1 \\ T_2 \\ T_3 \\ T_4 \\ T_5 \\ T_6 \end{bmatrix} = \begin{bmatrix} c_{1,1} & c_{1,2} & c_{1,3} & c_{1,4} & c_{1,5} & c_{1,6} \\ c_{2,1} & c_{2,2} & c_{2,3} & c_{2,4} & c_{2,5} & c_{2,6} \\ c_{3,1} & c_{3,2} & c_{3,3} & c_{3,4} & c_{3,5} & c_{3,6} \\ c_{4,1} & c_{4,2} & c_{4,3} & c_{4,4} & c_{4,5} & c_{4,6} \\ c_{5,1} & c_{5,2} & c_{5,3} & c_{5,4} & c_{5,5} & c_{5,6} \\ c_{6,1} & c_{6,2} & c_{6,3} & c_{6,4} & c_{6,5} & c_{6,6} \end{bmatrix} \begin{bmatrix} S_1 \\ S_2 \\ S_3 \\ S_4 \\ S_5 \\ S_6 \end{bmatrix} \tag{2.30}$$

For isotropic materials the matrix $\bar{c}_{ij}$ becomes [20]:

$$\bar{c}_{ij} = \begin{bmatrix} \lambda + 2\mu & \lambda & \lambda & 0 & 0 & 0 \\ \lambda & \lambda + 2\mu & \lambda & 0 & 0 & 0 \\ \lambda & \lambda & \lambda + 2\mu & 0 & 0 & 0 \\ 0 & 0 & 0 & \mu & 0 & 0 \\ 0 & 0 & 0 & 0 & \mu & 0 \\ 0 & 0 & 0 & 0 & 0 & \mu \end{bmatrix} \tag{2.31}$$

where λ and μ are the Lamè coefficients given in equation (2.18) and (2.19).

2.2 Wave theory

All theory presented in this section is based on information found in the books "Fundamentals of physical acoustics" [3], "The science and applications of acoustics" [25], "Fundamentals and Applications of ultrasonic waves" [7] and the Master thesis "Ultrasound sensor for biomedical applications" [2].

A wave can be described as the movement of a disturbance through a material or vacuum. The wave travels with a finite speed c_0, with respect to the medium in which it propagates. Although waves are often thought of as continuous sinusoidal oscillations, a waveform can take the form of spikes such as the delta function, rectangular pulses like the discontinuous unit step function, complex exponential- and logarithmic functions, and noise. Actually, all functions on the form $u = f(x - ct) + g(x + ct)$ satisfies the wave equation [3].

Sound waves are longitudinal pressure waves, which means that the particles in the medium oscillate back and forth in the direction of the wave, creating alternating compressions and rarefactions in the material. Sound waves therefore needs a medium to propagate. Electromagnetic waves however, such as light and radio waves, can travel through vacuum.

Mathematically the three dimensional wave equation is given by [3]:

$$c_0^2 \nabla^2 u(x, y, z, t) - \frac{\delta^2 u}{\delta t^2} = 0 \tag{2.32}$$

where u is the waveform and nabla ∇ is the Laplace operator given by:

$$\nabla^2() = \frac{\delta^2}{\delta x}() + \frac{\delta^2}{\delta y}() + \frac{\delta^2}{\delta z}() \tag{2.33}$$

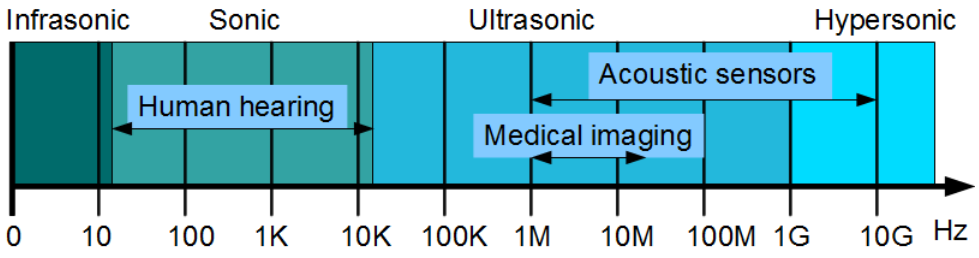

Figure 2.5: The acoustic frequency spectrum [7] [2].

Sound waves with frequencies between 20 KHz and 1 GHz are called ultrasonic waves. That is, frequencies right above the human hearing and up to the hypersonic regime [7] [2]. Figure 2.5 shows a drawing of the acoustic frequency spectrum.

2.2.1 Wave equation for fluids

Since this thesis evolves around acoustical ultrasonic waves, it will suffice to derive the wave equation in 1-D. We limit the problem by applying a lossless plane wave, which leads us to only need the 1-D conservation equations for non-dissipative fluids. We also neglect all body forces, such as gravity [3].

To derive the wave equation, we first consider the conservation of mass. Then we take a look at the conservation of momentum and the equation of state, before finally arriving at the wave equation.

Conservation of mass

We start by considering a compressible fluid that flows through a duct with some arbitrary, but uniform cross section area S. Such a duct is shown in Figure 2.6, where x and Δx marks the boundaries of a infinitesimal control volume. The fluid runs through the control volume with the particle velocity u, and we want to find out at which rate the mass inside changes. To begin with, we make two assumptions [3]:

1. The position of the control volume is fixed in space
2. The fluid has 1-D flow

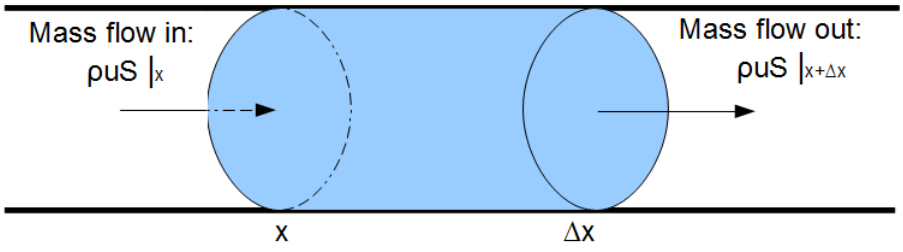

Figure 2.6: Mass flow through a control volume [3].

Since we assume 1-D flow, it follows that all the flow properties, such as the particle velocity u and the fluid density ρ, are the same throughout any cross section of the control volume. Because of the conservation of mass, we know that the total fluid mass inflow must equal the total fluid mass outflow. In mathematical notation this is the same as [3]:

$$\frac{\delta}{\delta t}(S\rho\Delta x) = \rho uS|_x - \rho uS|_{x+\Delta x} \tag{2.34}$$

where ρ on the left side represents the average fluid density inside the control volume. Because neither the area S nor Δx is dependent on time, we can rewrite equation (2.34) to:

$$\frac{\delta}{\delta t} = \frac{\rho u|_x - \rho u|_{x+\Delta x}}{\Delta x} \tag{2.35}$$

Letting $\Delta x \to 0$, we see that the right side of equation (2.35) becomes $-\frac{\delta \rho u}{\delta x}$, where the density ρ is a true point function. The equation of continuity for conservation of mass follows directly [3]:

$$\frac{\delta}{\delta t} + \rho\frac{\delta u}{\delta x} \tag{2.36}$$

Conservation of momentum

Figure 2.7 shows the same control volume as applied for the derivation of the equation of continuity. ρu is the momentum per unit volume, and $\rho u^2 S$ is the momentum flux (units; momentum per unit area per unit time).

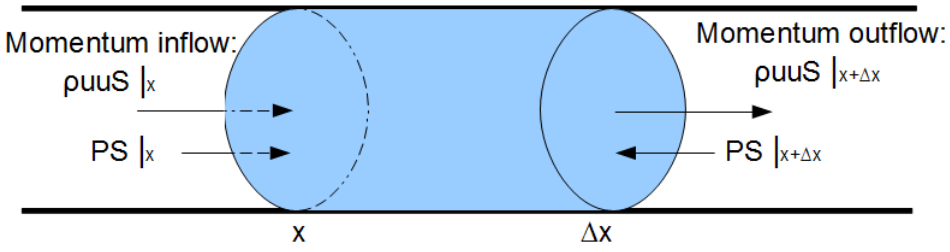

Figure 2.7: Momentum flow through- and forces on a control volume [3].

To find a momentum balance relation, we start by expanding the list of assumptions used above by another two points [3]:

1. The position of the control volume is fixed in space
2. The fluid has 1-D flow
3. Neglect all body forces, as they are not significant at infinitesimal distances
4. Assume inviscid fluid; the pressure P gives the only significant surface force

Assuming that these four points are true, the forces $PS|_x$ and $PS|_{x+\Delta x}$ are the only ones acting on the control volume. The pressure P is the sum of the acoustic and ambient pressure on the boundary area S. If we now write Newton's second law in terms of momentum conservation we get:

$$\frac{\delta}{\delta t}(\rho u S \Delta x) = (\rho u^2 S|_x - \rho u^2 S|_{x+\Delta x}) + (PS|_x - PS|_{x+\Delta x}) \tag{2.37}$$

which with words means that the time rate momentum increase inside the control volume equals the total momentum inflow over the boundaries plus the sum of all the forces acting on the control volume [3]. By dividing equation (2.37) with $S\Delta x$, and rearranging we get:

$$\frac{\delta}{\delta t}(\rho u) + \frac{\rho u^2 S|_{x+\Delta x} - \rho u^2|_x}{\Delta x} + \frac{P|_{x+\Delta x} - P|_x}{\Delta x} = 0 \tag{2.38}$$

Finally, if we let $\Delta x \to 0$, equation (2.38) becomes

$$\frac{\delta}{\delta t}(\rho u) + \frac{\delta \rho u^2}{\delta x} + \frac{\delta P}{\delta x} = 0 \tag{2.39}$$

which is known as the momentum equation [3].

Equation of state

Still considering the control volume from the previous sections, we begin the derivation of the isentropic equation of state by adding another necessary point to our list of assumptions:

1. The position of the control volume is fixed in space
2. The fluid has 1-D flow
3. Neglect all body forces, as they are not significant at infinitesimal distances
4. Assume inviscid fluid; the pressure P gives the only significant surface force
5. Lossless flow

Because we assume that the flow is lossless, there is no need for any separate equation for conservation of energy. It therefore suffices to consider the thermodynamic equation of state, which mainly is a relation between thermodynamic variables. Generally, the equation of state $P = P(\rho, s)$ is useful in acoustics - relating pressure to density and the entropy s per unit mass. However, because of our assumption of the flow being lossless, the entropy becomes constant and the pressure P becomes only a function of density:

$$P = P(\rho) \tag{2.40}$$

which is a general form of the isentropic equation of state.

This can be expressed by a Taylor series in the condensation of $\frac{\rho-\rho_0}{\rho_0}$ for any fluid, be it liquid or gas [3]:

$$P = p_0 + A\left(\frac{\rho-\rho_0}{\rho_0}\right) + \frac{B}{2!}\left(\frac{\rho-\rho_0}{\rho_0}\right)^2 + \frac{C}{3!}\left(\frac{\rho-\rho_0}{\rho_0}\right)^3 + (...) \tag{2.41}$$

where p_0 and ρ_0 are the static values of P and ρ, respectively. The coefficients A, B and C are estimated through experiments or by other types of analysis. The first coefficient is the most important because the condensation generally is very small. The speed of sound c is defined by [3]:

$$c^2 = \frac{\delta P}{\delta \rho}|_{const.s} = \frac{dP}{d\rho} \tag{2.42}$$

for an isentropic process. By taking the limit $\rho \to \rho_0$, and differentiating equation (2.41), c^2 becomes

$$c_0^2 = \frac{A}{\rho_0} \tag{2.43}$$

which is known as the "small-signal sound speed", or more traditionally only "Sound speed". Eliminating the condensation terms from the pressure, P in equation (2.41) simplifies the to the "acoustic" or "excess pressure" p as given by equation (2.44). Equation (2.45) gives the excess density [3].

$$p \equiv P - p_0 \tag{2.44}$$

$$\delta\rho \equiv \rho - \rho_0 \tag{2.45}$$

The isentropic equation of state can then be written as [3]:

$$p = c_0^2 \delta\rho \left[1 + \frac{B}{2!A}\frac{\delta\rho}{\rho_0} + \frac{C}{3!A}\left(\frac{\delta\rho}{\rho_0}\right)^2 + (...)\right] \tag{2.46}$$

Resulting wave equation

The previous sections give us all the tools we need to derive the 1-D wave equation for a lossless homogenous fluid. We will use the equation of continuity (2.36), the momentum equation (2.39) and the isentropic equation of state (2.46) to derive the wave equation. These three equations are all non-linear, but by using "small signal approximation" they can be linearized.

We start by assuming that the fluid is silent in the absence of sound waves, which gives us that the pressure $P = p_0$, the density $\rho = \rho_0$ and the particle velocity $u = 0$. Assuming that the sound waves only disturb the equilibrium of the fluid marginally, gives us that the excess pressure p, the excess density $\delta\rho$ and the particle velocity u are all small quantities of first order. This means that we can assume that these variables are all small compared to the static quantities p_0, ρ_0 and c_0 as:

$$|\delta\rho| << \rho_0 \tag{2.47}$$

$$|p| << \rho_0 c_0^2 \tag{2.48}$$

$$|u| << c_0 \tag{2.49}$$

The two equations (2.48) and (2.49) follow directly from equation (2.47). Applying a "small signal approximation" simply means to use these assumptions [3].

To get to the wave equation, we use the small signal approximations to linearize the conservation equations in (2.36), (2.39) and (2.46). Next we can combine them to obtain the linear wave equation [3]:

$$c_0^2 \frac{\delta^2 u}{\delta x^2} - \frac{\delta^2 u}{\delta t^2} = 0 \tag{2.50}$$

A general solution to the wave equation can be expressed by

$$p(x,t) = \Lambda e^{j(\omega t - kx)} \tag{2.51}$$

where Λ represents the amplitude, ω the angular frequency and k the wave number.

2.2.2 Wave equation in elastic materials

Another approach to derive the 1-D wave equation, is to use an elastic material as the propagation medium instead of the homogeneous fluid used in the section above. We will still limit ourselves to the 1-D case. To derive the wave equation, we use Newton's second law as given by equation

(2.52), and a 1-D version of Hooke's law which is given in its general form by equation (2.20) in section 2.1.4.

Newton's second law is given by [20] [17]:

$$F = ma_1 = \rho_0 \frac{\delta v_1}{\delta t} - \frac{\delta T_1}{\delta x} \tag{2.52}$$

where m is the mass and ρ_0 is the density of the material, a_1 and v_1 is the displacement velocity -and acceleration of the wave, respectively, and T_1 is the stress given by [20]:

$$T_1 = c_E S_1 = c_E \frac{\delta u_1}{\delta x} \tag{2.53}$$

This is Hooke's law in 1-D, where c_E is the elastic modulus, u_1 is the displacement and S_1 is the strain defined in equation 2.8 in section 2.1.2.

We recall that $v_1 = \frac{\delta u_1}{\delta t}$, and start by taking the time derivative of Hooke's law from equation (2.53):

$$\frac{\delta T_1}{\delta t} = c_E \frac{\delta}{\delta t}\left(\frac{\delta u_1}{\delta x}\right) = c_E \frac{\delta}{\delta x}\left(\frac{\delta u_1}{\delta t}\right) = c_E \frac{\delta v_1}{\delta x} \tag{2.54}$$

Next, we take the time derivative of Newton's second law from equation (2.52) and use our result from equation (2.54), which leads us to:

$$\frac{\delta F}{\delta t} = \frac{\delta}{\delta t}\left(\rho_0 \frac{\delta v_1}{\delta t} - \frac{\delta T_1}{\delta x}\right) = \rho_0 \frac{\delta^2 v_1}{\delta t^2} - \frac{\delta}{\delta x}\left(\frac{\delta T_1}{\delta t}\right) = \rho_0 \frac{\delta^2 v_1}{\delta t^2} - \frac{\delta}{\delta x}\left(c_E \frac{\delta v_1}{\delta x}\right)$$
$$\frac{\delta F}{\delta t} = \rho_0 \frac{\delta^2 v_1}{\delta t^2} - c_E \frac{\delta^2}{\delta x^2} \tag{2.55}$$

Finally, by rearranging equation (2.55) we find the wave equation [20]:

$$\frac{\delta^2 v_1}{\delta t^2} = \frac{c_E}{\rho_0} \frac{\delta^2 v_1}{\delta x^2} = c_0^2 \frac{\delta^2 v_1}{\delta x^2} \tag{2.56}$$

where c_0 is the phase velocity.

2.3 Attenuation in thick polymer samples

2.3.1 Direct signal

When there is only water between the transducers, the frequency spectrum of the received signal can be described by equation (2.57) [14]. A sketch of the setup is shown in Figure 2.8.

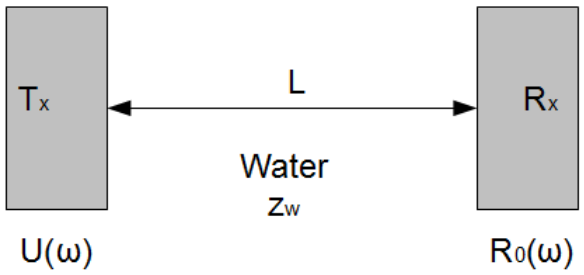

Figure 2.8: System without polymer sample inserted.

$$R_0(\omega) = e^{-ik_w L}\, U(\omega) \tag{2.57}$$

where $U(\omega)$ is the frequency spectrum of the original signal that was sent from the transducer T_x, and L is the distance between the transducers as shown in Figure 2.8. $k_w(\omega)$ is the wave number for water, given by [31]:

$$k_w(\omega) = \alpha_w(\omega) - i\beta_w(\omega) \tag{2.58}$$

where α_w and β_w are the propagation constant and the attenuation coefficient for water, respectively. Inserting into equation (2.57) gives a complex propagation constant, which is canceled by taking the absolute value of the spectrum:

$$R_0(\omega) = e^{-i(\alpha_w - i\beta_w)L}\, U(\omega) = e^{-\beta_w L}\, e^{-i\alpha_w L}\, U(\omega) \tag{2.59}$$

$$|R_0(\omega)| = e^{-\beta_w L}\, |U(\omega)| \tag{2.60}$$

2.3.2 Transmission through a thick polymer sample

A drawing of the system when a polymer sample is inserted between the transducers is given in Figure 2.9. The Fourier transform $R_1(\omega)$ of the received signal with this setup is given by [14]:

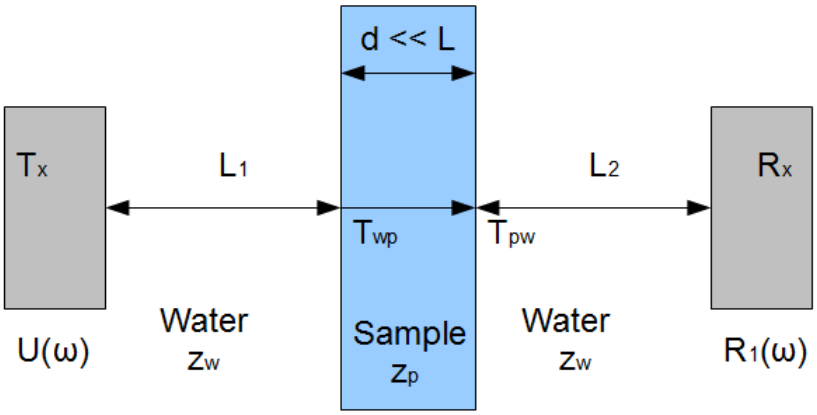

Figure 2.9: System with a polymer sample inserted.

$$R_1(\omega) = e^{-ik_w L_2}\, T_{pw}\, e^{-ik_p d}\, T_{wp}\, e^{-ik_w L_1}\, U(\omega) = T\, e^{-ik_w(L-d)}\, e^{-ik_p d}\, U(\omega) \tag{2.61}$$

$$k_p(\omega) = \alpha_p(\omega) - i\beta_p(\omega) \tag{2.62}$$

where L_1 is the distance between the sending transducer and the sample, L_2 is the distance between the sample and the receiving transducer and d is the thickness of the polymer sample as indicated by Figure 2.9, such that $L_1 + L_2 + d = L$. The distances L_1 and L_2 are equal, and are chosen according to the focus length of the transducers, such that the sample is in the center of focus.

$k_p(\omega)$ is the wave number with α_p and β_p as the propagation constant and the attenuation coefficient for the inserted polymer sample, respectively. T_{wp} and T_{pw} are the transmission coefficients for the two interfaces involved, as indicated by Figure 2.9. When the material that the signal is transmitted into is assumed to have an infinite thickness, the equations for the transmission coefficients are given by [3]:

$$T_{wp} = \frac{2z_p}{z_w + z_p}, \quad T_{pw} = \frac{2z_w}{z_w + z_p} \tag{2.63}$$

where z_w and z_p are the impedances of water and the polymer, respectively. The impedance of a

material m is defined as [6]:

$$z_m = \rho_m c_m \tag{2.64}$$

where ρ_m the density and c_m is the sound velocity of the material.

T is the total transmission coefficient for a material; it is defined as the product between T_{wp} and T_{pw}. Still assuming that the second medium has infinite thickness, T is given by:

$$T = T_{wp} \cdot T_{pw} = \frac{4 z_w z_p}{(z_w + z_p)^2} \tag{2.65}$$

When the thickness of the inserted sample is large compared to the wavelength, equation (2.65) can be used as an approximation of the total transmission coefficient.

By taking the absolute value of the frequency spectrum in equation (2.61), the complex propagation constants for water and the polymer specimen is eliminated:

$$\begin{aligned} |R_1(\omega)| &= |T| \; e^{-\beta_w (L-d)} \; e^{-\beta_p d} \; |U(\omega)| \\ &= |T| \; e^{-L\beta_w} \; e^{-d(\beta_p - \beta_w)} \; |U(\omega)| \end{aligned} \tag{2.66}$$

2.3.3 Amplitude Spectrum

To find the total transmission coefficient T and the attenuation β_p through the polymer sample, we first select a frequency interval $\Delta\omega$ that covers the information bandwidth of the first peak in the frequency spectrum. The interval must be chosen above the noise floor. The radian frequencies in this interval will be denoted by ω'.

The next step is to take the ratio $A_1(\omega')$ between the absolute values of the frequency spectra at the interval $\Delta\omega$ of the received signal, with and without the polymer sheath inserted [18] [28]:

$$A_1(\omega') = \frac{|R_1(\omega')|}{|R_0(\omega')|} = \frac{|T| \; e^{-L\beta_w} \; e^{-d(\beta_p - \beta_w)} \; |U(\omega')|}{e^{-L\beta_w} \; |U(\omega')|} = |T| \; e^{-d(\beta_p - \beta_w)} \tag{2.67}$$

Furthermore, the phase spectrum is obtained by taking the logarithm of the amplitude spectrum $A_1(\omega')$, and by using the logarithmic rule [26]:

$$\ln(A_1(\omega')) = \ln\left(|T| \; e^{-d(\beta_p - \beta_w)}\right) = \ln(|T|) - d(\beta_p - \beta_w) \tag{2.68}$$

From this we find the logarithm of the total transmission coefficient T, through the polymer sample. Further, the total transmission coefficient can be given for that specific polymer by taking the exponential of $\ln[|T|]$. From equation (2.68), the attenuation coefficient β_p through the polymer can easily be solved for:

$$\beta_p - \beta_w = \frac{1}{d} \left[\ln(|T|) - \ln(A_1(\omega')) \right] \tag{2.69}$$

$$\beta_p = \beta_w + \frac{1}{d} \left[\ln(|T|) - \ln(A_1(\omega')) \right] \tag{2.70}$$

Since the attenuation through water is much smaller than the attenuation through the sample ($\beta_w << \beta_p$), the attenuation β_w of water can be ignored. Therefore, the attenuation through the sample can be calculated as given by [14]:

$$\beta_p \approx \beta_p - \beta_w = \frac{1}{d} \left[\ln(|T|) - \ln(A_1(\omega')) \right] \tag{2.71}$$

2.3.4 Neper to Decibel

Decibels is a common unit to use in acoustics. To convert the amplitude spectrum from Neper to Decibels we use the that [5]:

$$A_1(\omega') \ [dB] = 20 \log(\ln[A_1(\omega')]) \ [Np] \tag{2.72}$$

Applying this relation on equation (2.68) yields:

$$20 \log(\ln[A_1(\omega')]) = 20 \log(T) - d(\beta_p - \beta_w) 20 \log(e^1) \tag{2.73}$$

From this it is clear that to convert the damping factor β into units of dB/cm MHz, we simply multiply by the factor

$$20 \log(e^1) = 8.68 \tag{2.74}$$

2.3.5 Wave model with no dispersion

The phase velocities a_w in water and a_p in the polymer sample are given by [20]:

$$a_w = \frac{\omega}{k_w}, \quad a_p = \frac{\omega}{k_p} \tag{2.75}$$

where ω is the angular frequency, and k_w and k_p are the wave numbers of water and the sample respectively.

By assuming that the phase velocity is related to the speed of sound through the materials, we obtain the expressions for the loss factors δ_w through water, and δ_p through the polymer sample:

$$a_w = c_w(1 + i\delta_w), \quad a_p = c_p(1 + i\delta_p) \tag{2.76}$$

$$|\delta_w| << 1, \quad |\delta_p| << 1 \tag{2.77}$$

where c_w is the speed of sound in water and c_p is the speed of sound through the polymer sample [20].

We can then use these assumptions and solve equation (2.75) for the wave numbers, to relate them to the loss factor and the attenuation coefficient as shown for k_w as:

$$k_w = \frac{\omega}{a_w} = \frac{\omega}{c_w(1 + i\delta_w)} \approx \frac{\omega}{c_w}(1 - i\delta_w) \tag{2.78}$$

Thus, since $k_w = \alpha_w - i\beta_w$, we get that $\alpha_w - i\beta_w \approx \frac{\omega}{c_w}(1 - i\delta_w)$. The equivalent relation yields for the wave number k_p. This results in the propagation constants and the attenuation coefficients given by [20]:

$$\alpha_w = \frac{\omega}{c_w}, \quad \alpha_p = \frac{\omega}{c_p} \tag{2.79}$$

$$\beta_w = \frac{\omega}{c_w}\delta_w, \quad \beta_p = \frac{\omega}{c_p}\delta_p \tag{2.80}$$

If the speed of sound is not dependent on frequency, then the spectrum ratio $A_1(\omega')$ is given by [20]:

$$A_1(\omega') \approx |T|\ e^{-d\beta_p} = |T|\ e^{-d\frac{\omega}{c_p}\delta_p} \tag{2.81}$$

To obtain the loss factor δ_p of the polymer, the first step is to take the logarithm of $A_1(\omega')$ in

equation (2.81):

$$\ln\left(\frac{A_1(\omega')}{|T|}\right) = -d\frac{\omega}{c_p}\delta_p \tag{2.82}$$

Then we use that the angular frequency ω is related to the frequency f by $\omega = 2\pi f$ to get:

$$\ln\left(\frac{A_1(\omega')}{|T|}\right) = -d\ \frac{2\pi f}{c_p}\ \delta_p \tag{2.83}$$

Next, if we use the logarithmic rule of that $\ln\left(\frac{A_1(\omega')}{|T|}\right) = \ln(A_1(\omega')) - \ln(|T|)$, and solve equation (2.83) for $\delta_p f$ we obtain

$$\begin{aligned} &-\frac{c_p}{2\pi d}\ [\ \ln(A_1(\omega')) - \ln(|T|)\ ] = \delta_1 f \\ \Rightarrow\quad &f_0\ [\ \ln(|T|) - \ln(A_1(\omega'))\ ] = \delta_p f \end{aligned} \tag{2.84}$$

Finally, by using $y = -f_0 \ln(A_1(\omega'))$ and $y_0 = -f_0 \ln(|T|)$ in equation (2.84) we get:

$$y - y_0 = \delta_p f \tag{2.85}$$

Thus, the loss factor through the polymer sample can be expressed by [20]:

$$\delta_p = \frac{y - y_0}{f} = \frac{y}{f} - \frac{y_0}{f} \tag{2.86}$$

2.4 Attenuation in thin polymer samples

When the thickness of the sample is very thin compared to the wavelength, the theory of total transmission given in subsection 2.3.2 no longer applies. This is because the first echo to reach the receiving transducer no longer can be separated from the ringing inside the sample. The following theory is based on the book "Fundamentals of physical acoustics" [3].

We start by assuming that material 2 in Figure 2.10 has a finite thickness d. The pressure fields

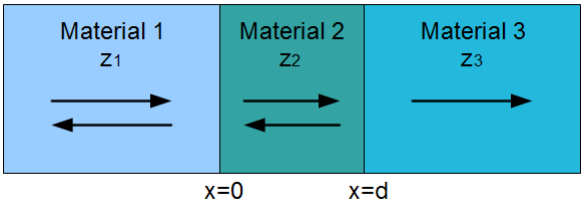

Figure 2.10: Two interface system with incident wave, reflected waves and transmitted waves [3].

P_1, P_2 and P_3 in the three materials in the system are given by [3]:

$$P_1 = A_1 e^{-ik_1 x} + B_1 e^{ik_1 x} \tag{2.87}$$

$$P_2 = A_2 e^{-ik_2 x} + B_2 e^{ik_2 x} \tag{2.88}$$

$$P_3 = A_3' e^{-ik_3 x} = A_3 e^{-ik_3 (x-d)} \tag{2.89}$$

where k_1, k_2 and k_3 are the wave numbers of the three materials, respectively, and A_3' is the amplitude with respect to the origin at $x = 0$. By using the continuity of pressure and particle velocity on the first interface , we can see that [3]:

$$A_1 + B_1 = A_2 + B_2 \tag{2.90}$$

$$A_1 - B_1 = \frac{z_1}{z_2}(A_2 - B_2) \tag{2.91}$$

where z_1 and z_2 are the impedances of the first and second materials involved as indicated in Figure 2.10. Continuity of pressure and particle velocity on the second interface give [3]:

$$A_2 e^{-ik_2 d} + B_2 e^{ik_2 d} = A_3 \tag{2.92}$$

$$A_2 e^{-ik_2 d} - B_2 e^{ik_2 d} = \frac{z_2}{z_3} A_3 \tag{2.93}$$

where z_3 is the impedance of the third material. To eliminate B_1, we add equation (2.91) to equation (2.90) and get:

$$2A_1 = \left(1 + \frac{z_1}{z_2}\right) A_2 + \left(1 - \frac{z_1}{z_2}\right) B_2 \tag{2.94}$$

To eliminate A_2 and B_2, we start by subtracting equation (2.93) from equation (2.92) to get:

$$2B_2 e^{ik_2 d} = \left(1 - \frac{z_2}{z_3}\right) A_3 \tag{2.95}$$

and then adding equation (2.93) to equation (2.92) to obtain:

$$2A_2e^{-ik_2d} = \left(1 + \frac{z_2}{z_3}\right) A_3 \tag{2.96}$$

The three equations (2.94), (2.95) and (2.96) can be combined to find that:

$$A_1 = \frac{A_3\left(\left(1+\frac{z_1}{z_2}\right)^2 e^{ik_2d} + \left(1-\frac{z_1}{z_2}\right)^2 e^{-ik_2d}\right)}{4} \tag{2.97}$$

Finally, we can find an expression for the total transmission coefficient T, which is defined as the ratio between A_3 and A_1:

$$T = \frac{A_3}{A_1} = \frac{4}{\left(1+\frac{z_2}{z_3}+\frac{z_1}{z_2}+\frac{z_1}{z_3}\right)e^{ik_2d} + \left(1-\frac{z_2}{z_3}-\frac{z_1}{z_2}+\frac{z_1}{z_3}\right)e^{-ik_2d}} \tag{2.98}$$

Using Euler's formulas, the total transmission coefficient is simplified to [3]:

$$T = \frac{2}{\left(1+\frac{z_1}{z_3}\right)\cos(k_2d) + i\left(\frac{z_2}{z_3}+\frac{z_1}{z_2}\right)\sin(k_2d)} \tag{2.99}$$

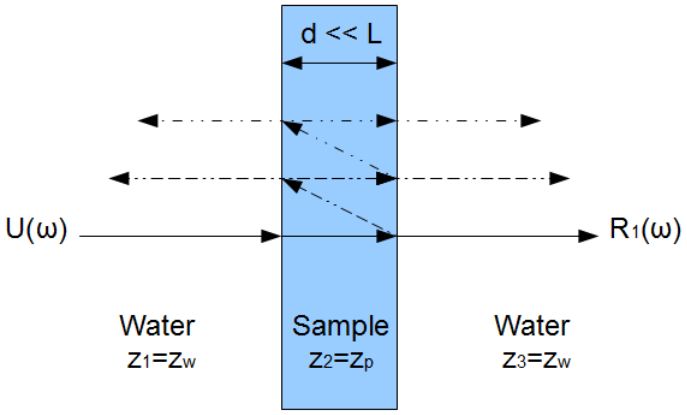

Figure 2.11: Reflections and transmission in a thin layer. The arrows do not show the actual wave paths.

When $z_1 = z_3$ as in Figure 2.11 where a thin polymer sample is enclosed by water, equation (2.99)

above reduces to:

$$T = \frac{2}{2\cos(k_p d) + i\left(\frac{z_p}{z_w} + \frac{z_w}{z_p}\right)\sin(k_p d)} \tag{2.100}$$

where k_p is the wave number and d is the thickness of the polymer sample. z_p and z_w are the impedances of the polymer and the water, respectively.

2.4.1 System fidelity factor

The system fidelity factor (SFF) is a normalized measure of the similarity between the shapes of two signals $R_a(t)$ and $R_b(t)$. We expect one of the signals, here $R_b(t)$, to be much lower in amplitude than the other. Because of this, a comparison that includes their magnitude is not necessary. We therefore normalize the signals as shown in equations (2.101) and (2.102), before cross-correlating them. This will give a comparison of their shape only [24].

The SFF is defined as the maximum value of the cross-correlation between the two normalized signals, as given by:

$$\widehat{R}_a(t) = \frac{R_a(t)}{\|R_a(t)\|} = \frac{R_a(t)}{\left[\int_{-\infty}^{-\infty} |R_a(t)|^2 \, dt\right]^{\frac{1}{2}}} \tag{2.101}$$

$$\widehat{R}_b(t) = \frac{R_b(t)}{\|R_b(t)\|} = \frac{R_b(t)}{\left[\int_{-\infty}^{-\infty} |R_b(t)|^2 \, dt\right]^{\frac{1}{2}}} \tag{2.102}$$

$$SFF = \max_n \int_{-\infty}^{-\infty} \widehat{R}_a(t)\widehat{R}_b(t+\tau)dt \tag{2.103}$$

As a result of the normalization, the value of the system fidelity factor will be between 0 and 1. A SFF of 0 means that the shape of the two signals have no similarity, whereas a SFF of 1 means that the two signals have identical shapes [24].

Chapter 3

Method

3.1 Experimental

3.1.1 General setup and procedure

A sketch of the general setup for the experiment is presented in Figure 3.1. The original setup used in the laboratory is shown in Figure 3.2. An overview listing all the instruments used is given in Table 3.1.

Two sets of focused transducers were used; one set designed to operate best around 10 MHz, and the other designed to work best at around 20 MHz. From now on they are referred to as the "10 MHz transducers" and the "20 MHz transducers", respectively.

Instruments

Instrument	**Producer**	**Series**
Oscilloscope	Agilent Technologies	InfiniiVision DSO-X 3024A
Signal Generator	Tektronix	AFG3102
Amplifier	Precition Acoustic LTD	Hydrophone Booster Amplifier

Table 3.1: List of applied instruments.

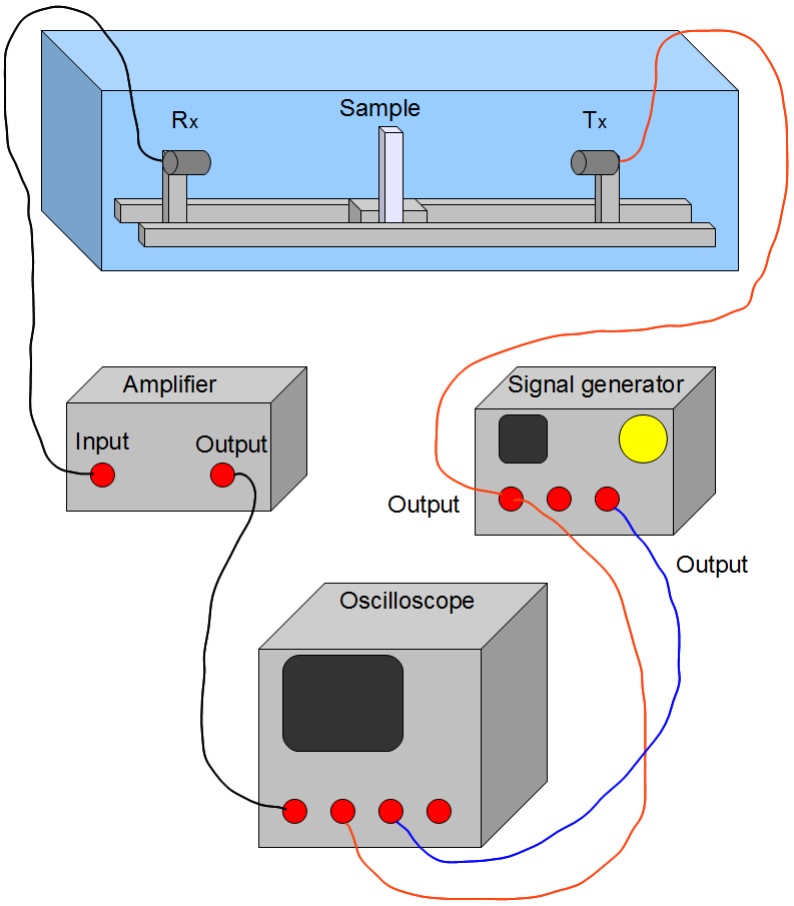

Figure 3.1: The setup used for the experiment.

To generate an appropriate waveform, the computer software "ArbExpress Application" was used. The waveform data file generated with this software was transmitted over to the signal generator only once. For all the experiments done in this thesis, a broadbanded modulated signal with 5 oscillations was defined and used. The equation of the waveform $U_e(t)$, as programmed on the computer, is given below with amplitude $V_0 = 5$ V and the number of oscillations $\gamma = 5$. Figure 3.3 shows the editor of the software as it was used.

$$U_e(t) = V_0 \cdot e^{-(t-\pi)^2} \cdot \sin(\gamma t) \tag{3.1}$$

For all the measurements, the voltage amplitude was amplified in the signal generator by a factor of 10 V peak to peak, the highest amplitude available. Since the amplitude of the waveform from

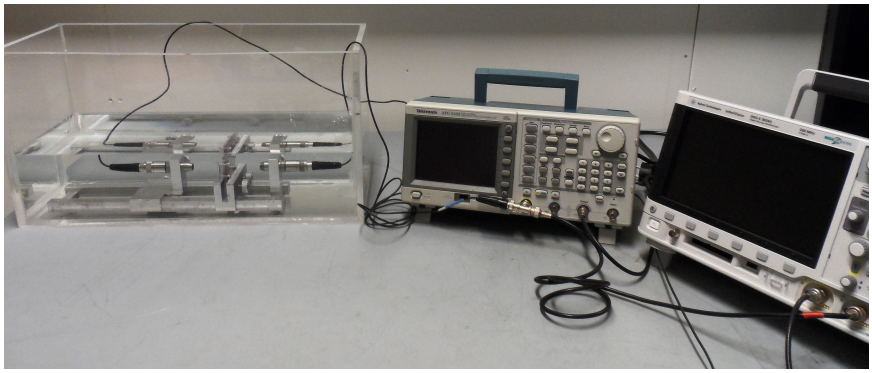

Figure 3.2: Image of the setup in the laboratory.

"ArbExpress Application" was 5 V, the overall voltage amplitude of the signal sent to the transducer was 50 V. The frequency of the signal was selected on the signal generator depending on which set of transducers that was applied.

Because $U_e(t)$ was sent to the signal generator, and then again passed on to the transmitting transducer T_x, the shape of the signal that was transmitted was unknown. The transmitted signal will therefore be referred to by $U(t)$.

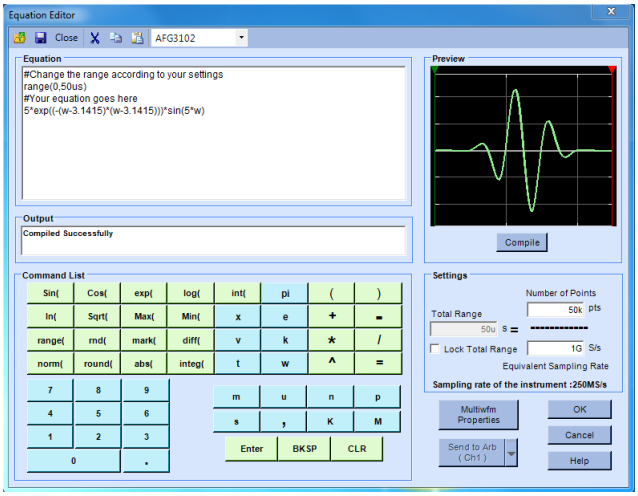

Figure 3.3: ArbExpress Application editor

Measurements were done both with and without a sample inserted between the transducers. The signal that only went through water will be referred to as the "direct signal" throughout this thesis. The inserted samples are discussed further in subsection 3.1.2 below.

The signal received by R_x was amplified and then shown on the oscilloscope as indicated in Figure 3.1. An appropriate time interval ΔT including the first echo was chosen manually on the oscilloscope, and then downloaded as a .csv file on a memory stick. Since all the time intervals were chosen manually to fit the first echo for each measurement, and because all the data-vectors taken from the oscilloscope had the same length, the sampling time Δt of each signal was varying depending on how the time intervals were selected.

3.1.2 Samples and material properties

Throughout the experiments, a total of six different obstacles were used. The polymers applied for the samples are listed in Table 3.2 with names and acronyms, together with some relevant material properties.

The impedances of the materials are defined as the product between the density ρ and sound velocity c of the material as given by equation (2.64) in section 2.3.2.

Polymer properties

Polymer	**Acronym**	**Density**	**Sound velocity**	**Impedance**
Polyetherimide (Ultem 1000)	PEI	1280 $\frac{kg}{m^3}$	2430 m/s	3.11 MRayls
Polymethyl-methacrylate	PMMA	1190 $\frac{kg}{m^3}$	2750 m/s	3.26 MRayls
Polycarbonate	PC	1180 $\frac{kg}{m^3}$	2270 m/s	2.69 MRayls
Polyimide (Kapton)	PI	1420 $\frac{kg}{m^3}$	2246 m/s	3.19 MRayls
Polyvinylidene-difluoride	PVDF	1780 $\frac{kg}{m^3}$	2140 m/s	3.81 MRayls

Table 3.2: Properties of different polymers used in the experiment.

The polymers will in general be referred to by their acronyms later in this thesis.

The properties for PMMA and PC were found in Appendix B of the book "Fundamentals and Applications of Ultrasonic waves" by Cheeke [7]. The same values were also found on the webpage NDTnet [21]. The type of PEI used in this experiment was Ultem 1000. The mass density of this polymer is given on the webpage K-mac Plastics [19]. The values for PVDF is found in the article "Experimental study of the acoustical properties of polymers utilized to construct PVDF ultrasonic transducers and the acousto-electric properties of PVDF and P(VDF/TrFE) films" [4]. The speed of sound and density for PI were found through simulations in COMSOL with Young's modulus E = 5.32 GPa and Poisson's ratio γ=0.3. These values were found in the article "Determination of

Young's modulus of thin films used in embedded passive devices" [10].

Table 3.3 lists some relevant properties for water at 20 °C. These properties were found in Appendix B in the book "Diagnostic Ultrasound Imaging" [30].

Water properties

Density	**Sound velocity**	**Impedance**	**Attenuation** β
1000 $\frac{kg}{m^3}$	1482 m/s	1.48 MRayls	0.002 dB/cm MHz

Table 3.3: Properties of water at 20 °C.

The six samples had different thicknesses as listed by Table 3.4. Obstacles 1-4 were samples consisting only of one polymer. Obstacle 5 and 6 were PI-films from the same shipment as obstacle 4, with a PVDF-coating spun manually on top. Because of the uncertainties originating from that the coating were spun on manually, the thickness of them were unknown in both cases. However, from the measurements presented below, we might assume that obstacle 2 (Sample 1) had an approximate coating thickness of 20 μm, and that the thickness of the coating of obstacle 6 (Sample 2) were approximately 10 μm.

Polymer thicknesses

Obstacle	**Material**	**Thickness**	**Uncertainty**
1	PEI	7.37 mm	± 40 μm
2	PMMA	8.06 mm	± 20 μm
3	PC	5.83 mm	± 20 μm
4	PI	130 μm	± 3 μm
5	Sample 1: PI, PVDF	150 μm	± 2 μm
6	Sample 2: PI, PVDF	137 μm	± 2 μm

Table 3.4: Thicknesses of the different polymer samples, with uncertainties; measured with a micrometer.

Because obstacles 1-3 in Table 3.4 were significantly thicker than obstacles 4-6, they will be referred to as the "thick samples", whereas obstacles 4-6 will be called the "thin samples" throughout this thesis. Since in addition the theory and setup applied for these two groups of samples had some differences, they are presented separately below.

Thick samples

For the three thick samples, PEI, PMMA and PC, measurements were done with both the 10 MHz- and the 20 MHz transducers. The temperature of the water in the tank while doing the experiments for the thick samples, varied from being 25.5 °C for the first measurements and falling towards 21.3 °C in the end.

These three samples were sufficiently thick to be attached directly to the slider on the framework. Figure 3.4 shows the three thick samples applied.

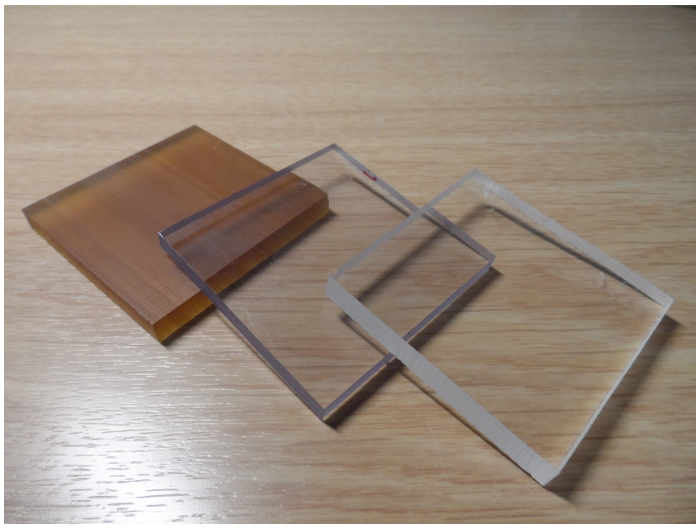

Figure 3.4: The thick samples. The closest sample is PMMA, the middle one is PC and the last is PEI.

Because the samples were several millimeters thick, we can assume that the transmission through the second interface is independent of the transmission through the first interface. The theory given by section 2.3 is therefore adequate for these samples.

Thin samples

For the three thin samples (PI-film and the two PVDF-coated PI-films), measurements were done only with the pair of 10 MHz transducers. The temperature of the water in the tank was regulated to keep around 20.5 °C throughout the experiment.

Unlike the thick samples described above, these samples could not be attached directly to the

framework without bending. Therefore, a frame made from polycarbonate was used to attach the films as straight as possible. During the measurements, the coating always faced the transmitting transducer, Tx. The thin samples are shown together with the frame in Figure 3.5.

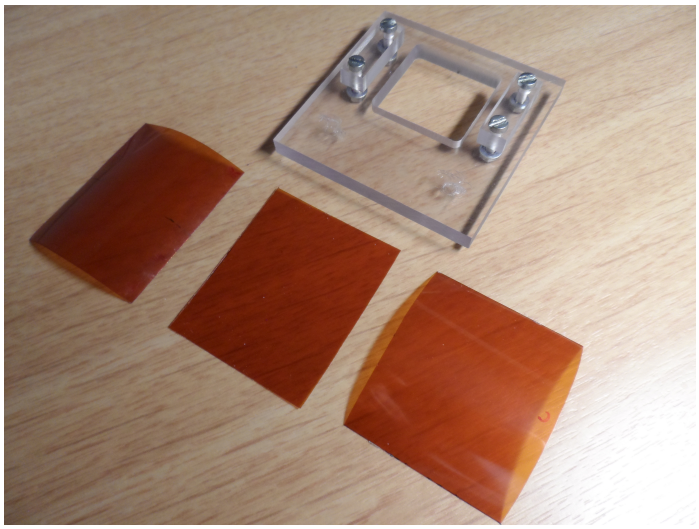

Figure 3.5: The thin samples and the frame. Sample 1 is to the left, the PI-film is in the middle, and Sample 2 is to the right.

Each of the coated samples were divided into two sides, as illustrated by Figure 3.6. On one side of the sample the surface of the PI was treated before the coating was spun on, while the surface on the other side of the sample was left untreated. The reason why the the samples were divided like this, was to make sure that the thickness of the coating became the same for the treated and untreated surfaces.

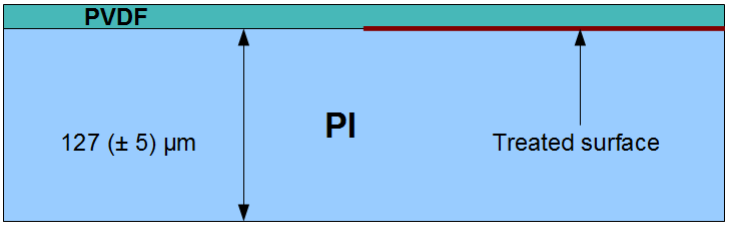

Figure 3.6: Illustration of a two-layer sample, where one side of the middle surface is treated and the other side is not.

Measurements were done through both of the sides separately to see if the surface treatment could

be detected, and whether or not it was useful. The method described above to spin the coating on would make comparison between the treated and untreated surfaces easier.

Throughout this thesis, the two sides of the coated samples will be referred to as the "left side" and the "right side" of the sample. Which side that was treated is unknown.

3.2 Numerical Simulations in COMSOL Multiphysics

COMSOL Multiphysics, hereafter referred to as COMSOL, is a computer software for simulating real-world scenarios through different kinds of physical models. It is a tool where you can easily build your own models by specifying a geometry, and selecting the required physics and meshing. The physics can be specified manually by the user, or chosen from a list of predefined materials and boundary conditions. The model is then ready to be solved for, to find the simulated scenario that the user needs. There are many options to choose from to display the solutions [9].

3.2.1 COMSOL models

Three models were made in COMSOL to simulate the environment in experiments: One model with only water between the transducers, one model with a PI-sample between the transducers and finally one model with a PVDF-coated PI-sample inserted. Figure 3.7 shows the right side of the 2-D axisymmetric model with PVDF-coated PI-film inserted. The two other models are not visualized here. This is because their only difference from Figure 3.7 was a removed coating for the measure through PI, and a completely removed obstacle for the simulation only through water.

The three models were all specified as listed beneath:

- **Space dimension:** 2-D Axisymmetric.
- **Physics:** Acoustic-Piezoelectric Interaction, Transient (acpztd).
- **Preset studies:** Time dependent.

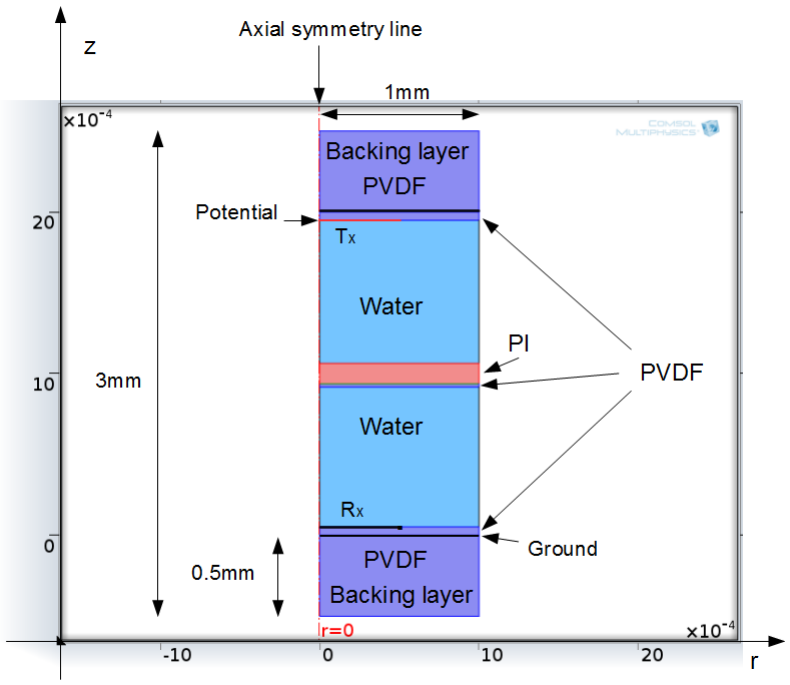

Figure 3.7: 2-D Model with PVDF-coated PI-film inserted.

The black lines in Figure 3.7 shows where the model was grounded. The horizontal red line shows where the potential was applied. The potential were implemented to have the same shape as the waveform programmed for the experiments, which is given in equation (3.1). To get a proper length of the waveform, the simulated pulse is given by:

$$U_n(t) = V_0 \cdot e^{-(ht-\pi)^2} \cdot \sin(k\gamma t) \tag{3.2}$$

where V_0 is the amplitude of the waveform, γ is the number of oscillations and h is a constant that scales the wavelength of the signal. h is calculated from the relation $h = \frac{2\pi f}{\gamma}$, which comes from the sine-term where one can see that $h\gamma = 2\pi f$. In these models the constants are defined corresponding to the experiments to be:

- V_0 =50 V
- γ =5
- f = 10 MHz
- $h = \frac{2\pi \cdot f}{5}$

We recall that in the experiments the waveform had to travel through both the signal generator and a physical transducer before being sent towards the receiving transducer. Therefore, the pulse $U(t)$ from the the experiments and the pulse $U_n(t)$ from the simulations, might not have exactly the same shape.

Figure 3.8 shows an image of the model in 3-D with a coated polymer film inserted when a pulse is being transmitted through.

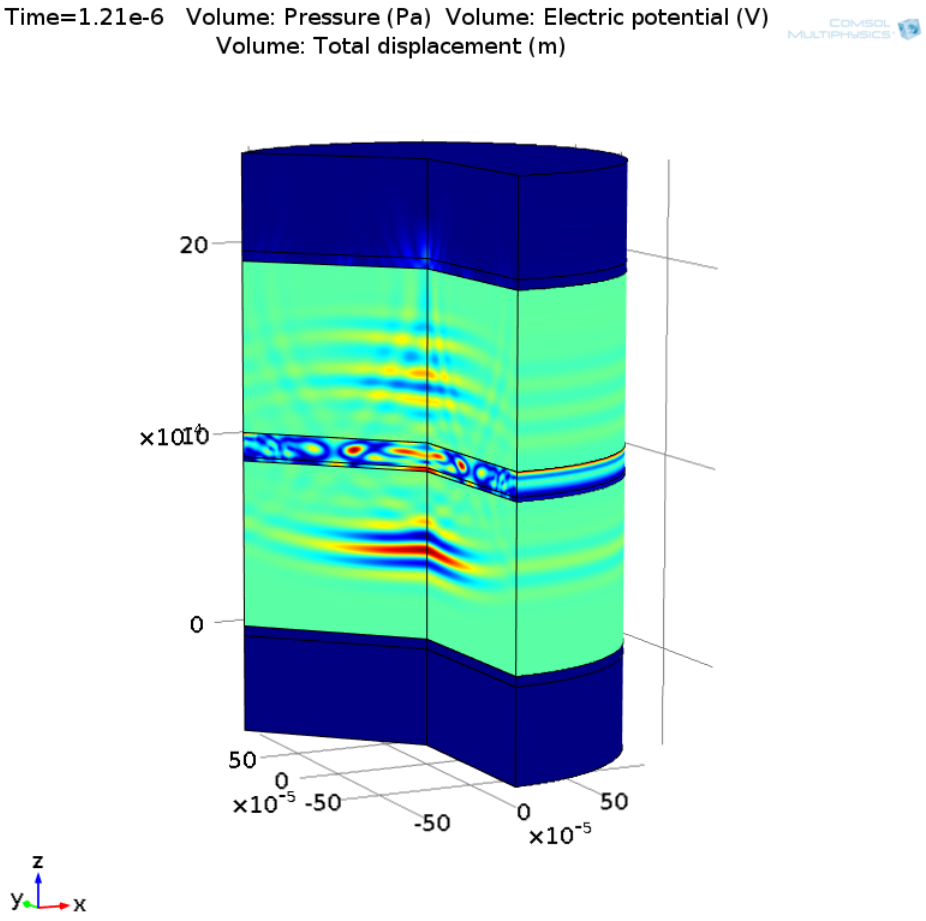

Figure 3.8: 3-D Model with PVDF-coated PI-film inserted.

Table 3.5 below lists the material properties applied in the COMSOL models, these properties were also used to make theoretical models. A short summary of the dimensions and materials with specifications that were used in the three models, are found in Table 3.6.

Material parameters for simulations.

Material	Sound velocity c	Density	Impedance
PI	2246 m/s	1420 $\frac{kg}{m^3}$	3.19 MRayls
PVDF	2400 m/s	1680 $\frac{kg}{m^3}$	4.03 MRayls
Water	1600 m/s	1000 $\frac{kg}{m^3}$	1.60 MRayls

Table 3.5: Material parameters applied in the simulations for transmission, these values were also used in the theoretical models.

COMSOL model

Part	Height	Width	Material	Specification
Backing layer	0.5 mm	2 mm	PVDF	Linear elastic material with Rayleigh damping
Transducer	52 μm	2 mm	PVDF	Piezoelectric material
Active transducer	1-D line	1 mm	PVDF	Electric potential/Ground
Sample	127 μm	2 mm	PI	Linear elastic material
Coating	10- or 20 μm	2 mm	PVDF	Linear elastic material
Water	1.896 mm	2 mm	Water	Model with only water
	1.769 mm	2 mm	Water	Model with sample
	1.859- or 1.849 mm	2 mm	Water	Model with coated sample

Table 3.6: Model specifications in COMSOL.

Backing layers with Rayleigh damping

As illustrated by Figure 3.7, a PVDF backing layer was applied on both the top and the bottom of the models. The purpose of the backing layers was to reduce reflections from the edges of the model. To do this, Rayleigh damping were defined in the material.

The Rayleigh damping factor C is defined in terms of the mass m and the stiffness k of the material as given by [13]:

$$C = \alpha m + \beta k \tag{3.3}$$

where α is the mass-proportional coefficient, and β is the stiffness-proportional damping coefficient.

To get a good value for the damping, a proper relative damping factor δ_E had to be chosen. δ_E is defined as the ratio between the actual and the critical damping. Next, two resonant frequencies ω_1 and ω_2 with the same relative damping factor δ_E had to be selected. The relative damping factor could then be related to the Rayleigh damping parameters α and β by the set of equations [13]:

$$\delta_E = \frac{1}{2}\left(\frac{\alpha}{\omega_1} + \beta\omega_1\right) \tag{3.4}$$

$$\delta_E = \frac{1}{2}\left(\frac{\alpha}{\omega_2} + \beta\omega_2\right) \tag{3.5}$$

From this we can derive expressions for the Rayleigh damping parameters as given by:

$$\alpha = \frac{\omega_1^2\omega_2 - \omega_1\omega_2^2}{\omega_1^2 - \omega_2^2}\ \delta_E \tag{3.6}$$

$$\beta = \frac{\omega_1 - \omega_2}{\omega_1^2 - \omega_2^2}\ \delta_E \tag{3.7}$$

For the this model the resonant frequencies f_1 and f_2 were chosen to be:

$$f_1 = 5\ MHz \tag{3.8}$$

$$f_2 = 15\ MHz \tag{3.9}$$

so that $\omega_1 = 2\pi f_1$ and $\omega_2 = 2\pi f_2$. The relative damping factor was selected to be:

$$\delta_E = 0.32 \tag{3.10}$$

3.3 Signal analysis

The analysis of the signals obtained experimentally and through simulations in COMSOL were done in MATLAB. Independent on whether the signal was produced through experiments or by simulations, they were analyzed by the same algorithm.

As previously explained in section 3.1.1, the the sampling time Δt of each experimentally received signal was varying depending on how the echoes were selected on the oscilloscope.

The speed of sound through each of the polymers is higher than the sound velocity in water. As a result, the first echo received by R_x for each of the measurements through a sample, did not overlap

in time with the direct signal. That is, when the waveform went through a polymer it reached R_x earlier than the waveform that only went through water. Therefore, the echoes had to be zero padded to overlap each other in time, before they could be interpolated to get the same sampling frequency. Consistently, the signal that went through a sample was the one being interpolated to match the direct signal.

The DC values of all the signals were also removed. This was done by calculating and subtracting the true mean of each of the signals. The same mean value was later used when zero padding the signals.

The Fourier transforms of the raw signals became quite coarse because the length of the original data vectors were too small. To smooth the spectra, the time dependent data was zero padded with 20 000 points [16].

3.3.1 Data analysis of thick samples

Equation (2.68) in section 2.3.3 suggests that the natural logarithm of the amplitude spectrum $A_1(\omega')$ should be a straight line. The linear relation between the ratio and the frequency is expected to exist only within an appropriate frequency interval Δf, of the frequency spectrum. At the edges of the spectrum, the relation is expected to loose its linearity due to lack of information in the signal and distortion from the noise floor.

As seen in equation (2.68) in section 2.3.3, the value of the amplitude spectra at DC is the logarithm of the total transmission coefficient T. Since the amplitude spectrum was only linear in Δf, the first order least squares method (LSM) was applied to the data in that interval to create a straight line that could cross DC. From this LS-line the total transmission coefficients and the damping factors of the thick materials could be estimated. The total transmission coefficient for the thick samples was found by taking the exponential of the value where the LS-line crossed DC. The damping factor β in units Np/cm MHz was found by calculating the slope of the LS-line, and converted into dB/cm MHz as described in section 2.3.4.

Since the estimation of total transmission coefficients and the damping factors were based on the LS-line that was fitted to the data in Δf, the definition of this interval had a direct influence on the results. The highest and lowest frequency defined for Δf were chosen manually by investigating the plots for where the data was linear.

In the results, the amplitude spectra data inside the frequency intervals Δf are plotted as black dots on top of their respective LS-lines. To get an impression of the real data, only every twentieth

data point was used to create the dots in the plot.

3.3.2 Data analysis of thin samples

The amplitude spectrum $A_1(\omega)$ for the received signal through the thin samples was obtained by taking the ratio between the frequency spectra as given by equation 2.67 in section 2.3.3.

In the case where a thin sample is inserted into water, as shown in Figure 2.11 in section 2.4, the amplitude spectrum given by equation (2.100) is expected to follow a periodic pattern with respect to frequency. Due to the distortions from the noise floor, the data are only expected to behave periodically in a frequency interval around the applied center frequency.

The transmission at resonant frequencies were found manually by investigating the spectrum.

The wave length of a signal is related to the sound velocity c, and the frequency f by [25]:

$$\lambda = \frac{c}{f} \tag{3.11}$$

The maxima of the amplitude spectra are found at the resonant frequencies. That is, when the length λ of the wave is related to the thickness d of the sample by [3]:

$$\lambda = \frac{2d}{n}, \quad n = 1, 2, 3... \tag{3.12}$$

By using the resonant frequencies f' at the maximums of the amplitude spectrum, the thickness of the sample can be estimated by:

$$\widehat{d} = \frac{n\lambda}{2} = \frac{nc}{2f'} \tag{3.13}$$

If the speed of sound through the material is unknown, we can find it by assuming that the first maximum is at $\lambda/2$ (where n=1), and apply the equations above to get that:

$$c = f' 2d \tag{3.14}$$

where f' is the first resonant frequency.

Chapter 4

Results

4.1 Experimental

4.1.1 Thick samples

Figure 4.1 shows the Fast Fourier transform of the received signals through the three thick polymer samples PEI, PMMA and PC, measured with two sets of transducers. Figure 4.2 shows the first order least-squares lines that fit the amplitude spectrum data from the three polymer samples, together with an illustration of the data as black dots.

Table 4.1 gives the total transmission coefficients T and the damping factors β of the three thick polymers obtained from the measurements done with the pair of 10 MHz transducers. The total transmission coefficients and damping factors for the thick polymers given in Table 4.2, are obtained through measurements with the set of transducers that function best around 20 MHz.

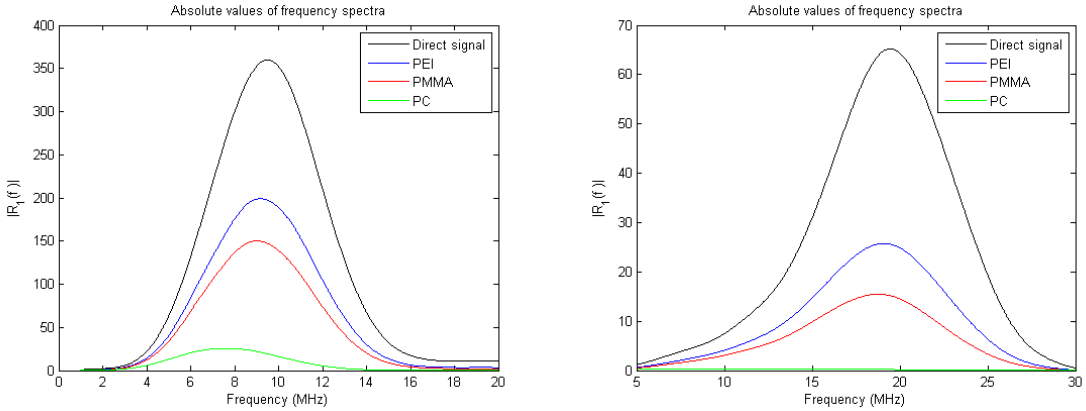

(a) 10 MHz transducers. (b) 20 MHz transducers.

Figure 4.1: Frequency spectrum from the directly received signal together, with the spectra for PEI, PMMA and PC. The signals were both sent with the optimal frequency for the applied transducers.

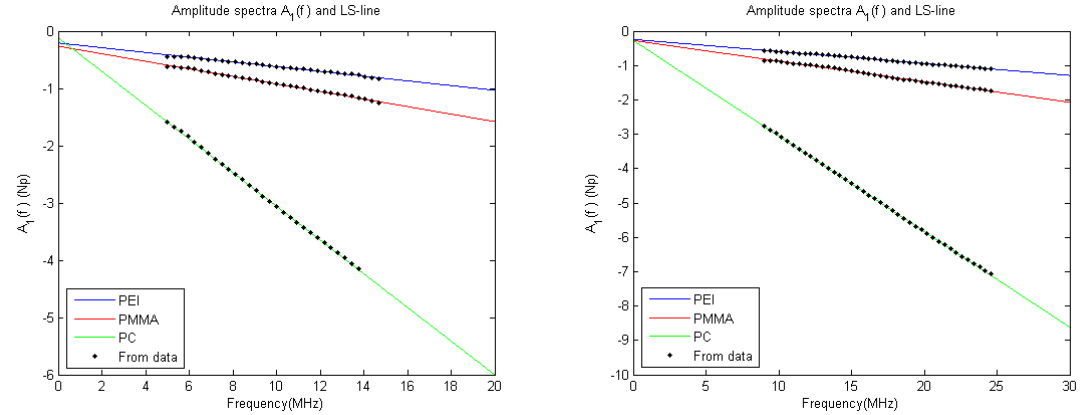

(a) 10 MHz transducers. (b) 20 MHz transducers.

Figure 4.2: Amplitude spectra for PEI, PMMA and PC obtained with two different sets of transducers. The black dots represents the data that the LSM was based on.

Total transmission coefficients and damping factors

Sample material	f_1	f_2	**T**	β **(dB/cm MHz)**
PEI	5	15	0.81	0.49
PMMA	5	15	0.77	0.71
PC	5	14	0.89	4.38

Table 4.1: Total transmission coefficients and damping factors found with the 10 MHz transducers. The lowest and highest frequency in the interval is called f_1 and f_2, respectively.

Total transmission coefficients and damping factors

Sample material	f_1	f_2	**T**	β **(dB/cm MHz)**
PEI	9	25	0.78	0.41
PMMA	9	25	0.76	0.64
PC	9	25	0.77	4.14

Table 4.2: Total transmission coefficients and damping factors found with the 20 MHz transducers. f_1 is the lowest frequency in the interval, and f_2 is the highest.

4.1.2 Thin samples

The results for Sample 1 and Sample 2 are presented separately. The waveforms, frequency spectrum and amplitude spectrum of the PI-film are plotted together with Sample 1 and Sample 2 in the following subsections.

Table 4.3 lists the values of the amplitude spectrum $A_1(f')$ at the frequencies f' for the PI-film, and estimates the thickness, $\widehat{d}$, of the film based on the theoretical speed of sound listed in Table 3.5 in section 3.2.1. An estimation for the speed of sound $\widehat{c}_{PI}$ in the PI-film is also presented.

Amplitude spectrum for PI-film through experiments

	First maximum	**Minimum**	**Second maximum**
$\mathbf{A_1(f')}$	0.98	0.74	0.92
f' [MHz]	8.67	13.20	16.65
λ **[μm]**	259	170	135
$\widehat{\mathbf{d}}$ **[μm]**	$\lambda/2 = 129$	$3\lambda/4 = 127$	$\lambda = 135$
$\widehat{\mathbf{c}}_{PI}$ **[m/s]**	2254		

Table 4.3: Transmission at resonance frequencies for the PI-film in Figure 4.4 and 4.6. Wavelength λ estimated by equation (3.11), sample thickness $\widehat{d}$ estimated by equation (3.13) with the speed of sound in PI from Table 3.5 in section 3.2.1. Estimated speed of sound $\widehat{c}_{PI}$ by equation (3.14)

.

Sample 1

Figure 4.3 shows the waveforms and frequency spectra of the received signals measured through both the left and right sides of Sample 1, together with those through the PI-sample and the directly received signal through water. Table 4.4 lists a number of shape-similarity comparisons of the waveforms in Figure 4.3a, in the form of several estimated System Fidelity Factors.

Figure 4.4 shows the amplitude spectra for the received signals through the left and right sides of Sample 1, together with the amplitude spectrum of the received signal through the PI-film.

Table 4.5 lists the values of the amplitude spectrum A_1(f') at the frequencies f' obtained through the left side of Sample 1, the corresponding values for the right side of Sample 1 are given by Table 4.6.

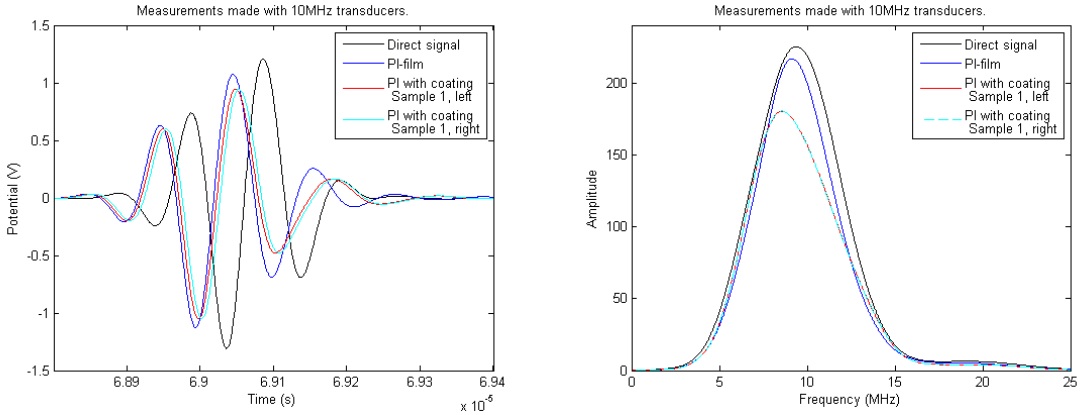

(a) Received waveform.

(b) Frequency spectra.

Figure 4.3: Waveforms and Fourier spectra for the received signals through water, PI and the left and right side of Sample 1.

System Fidelity Factors involving Sample 1

Signal a	**Signal b**	**System Fidelity factor**
PI-film	Direct signal	0.99
PI-film	Right, PVDF-coating	0.98
PI-film	Left, PVDF-coating	0.98
Right, PVDF-coating	Direct signal	0.99
Left, PVDF-coating	Direct signal	0.99
Left side coating	Right side coating	1.00

Table 4.4: System Fidelity Factors for waveforms received through Sample 1. "Signal a" is compared to "Signal b".

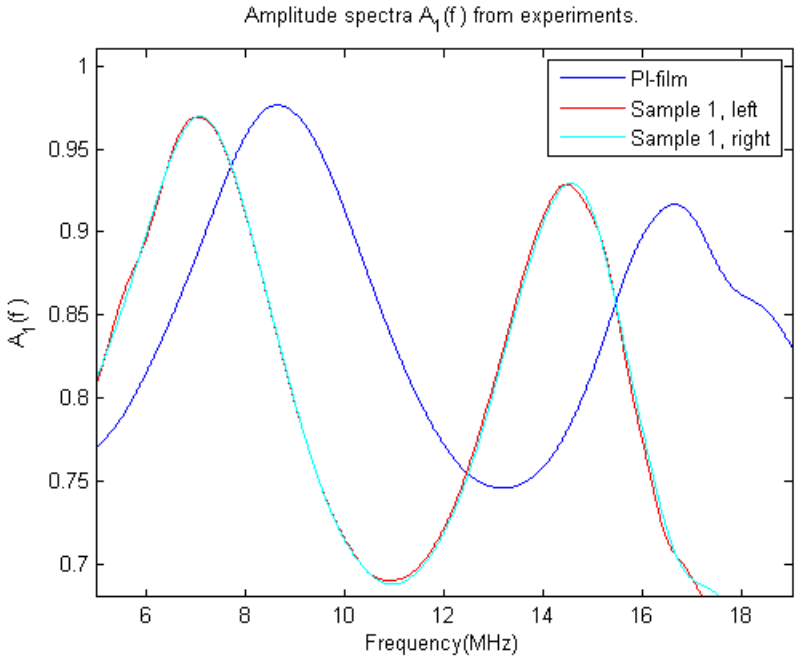

Figure 4.4: Experimentally obtained transmission through PI-film, and the left and right side of Sample 1.

Amplitude spectrum for the left side of sample 1 through experiments

	First maximum	**Minimum**	**Second maximum**
A_1(f')	0.97	0.69	0.93
f' [MHz]	7.05	10.91	14.46

Table 4.5: Transmission at resonance frequencies f' for the left side of Sample 1 in Figure 4.4.

Amplitude spectrum for the right side of sample 1 through experiments

	First maximum	**Minimum**	**Second maximum**
A_1(f')	0.97	0.69	0.93
f' [MHz]	7.10	10.97	14.56

Table 4.6: Transmission at resonance frequencies for the right side of Sample 1 in Figure 4.4.

Sample 2

The waveform and frequency spectra of both the left and right sides of Sample 2 are shown in Figure 4.5 together with waveforms and frequency spectra of the direct signal and the PI-film. Table 4.7 lists several estimated System Fidelity Factors for the waveforms shown in Figure 4.5a.

The amplitude spectra of the received signals through both the left and right side of Sample 2 are shown in Figure 4.6, together with the amplitude spectrum of the received signal through the PI-film.

Table 4.8 and 4.9 lists the values of the amplitude spectra at the frequencies f', for the received signals through the left and right side of Sample 2, respectively.

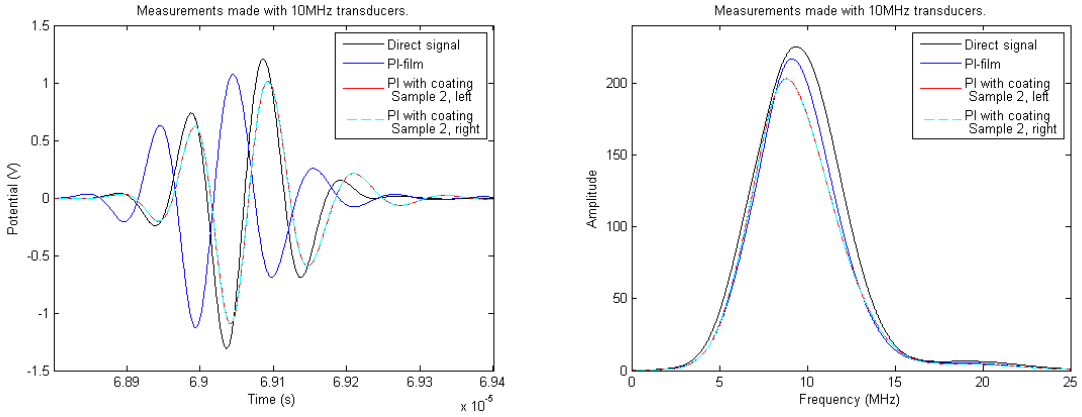

(a) Received waveform.

(b) Frequency spectra.

Figure 4.5: Waveforms and Fourier spectra for the received signals through water, PI and the left and right side of sample 2.

System Fidelity Factors involving Sample 2

Signal a	**Signal b**	**System Fidelity Factor**
PI-film	Direct signal	0.99
PI-film	Right, PVDF-coating	0.99
PI-film	Left, PVDF-coating	0.99
Right, PVDF-coating	Direct signal	0.99
Left, PVDF-coating	Direct signal	0.99
Left side coating	Right side coating	1.00

Table 4.7: System Fidelity Factors for waveforms obtained through Sample 2. "Signal a" is compared to "Signal b".

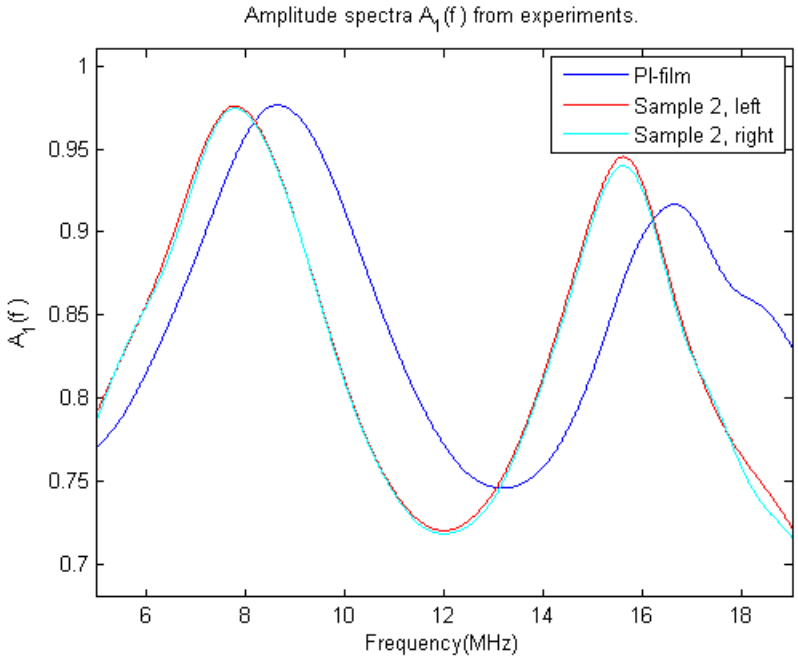

Figure 4.6: Experimentally obtained transmission through PI-film, and the left and right side of Sample 2.

Amplitude spectrum for the left side of Sample 2 through experiments

	First maximum	Minimum	Second maximum
A_1(f')	0.98	0.72	0.94
f' [MHz]	7.81	12.01	15.61

Table 4.8: Transmission at resonance frequencies for the left side of Sample 2 in Figure 4.6.

Amplitude spectrum for the right side of Sample 2 through experiments

	First maximum	Minimum	Second maximum
A_1(f')	0.97	0.72	0.94
f' [MHz]	7.81	12.02	15.61

Table 4.9: Transmission at resonance frequencies for the right side of Sample 2 in Figure 4.6.

4.2 Theoretical and numerical

4.2.1 Thick samples

Theoretical transmission

Table 4.10 gives theoretical values of the total transmission coefficients T for PEI, PMMA and PC. The estimations are based on the impedances of the polymers as listed in Table 3.2 and the impedance of water as given by Table 3.3 in section 3.1.1. The total transmission is estimated by equation (2.65) in section 2.3.2.

Calculated total transmission coefficients

Sample material	Total transmission T
PEI	0.87
PMMA	0.86
PC	0.91

Table 4.10: Calculated total transmission coefficients based on impedance.

4.2.2 Thin samples

The material properties listed in Table 3.5, and the sample thicknesses given by Table 3.6 in section 3.2.1, were applied to obtain both the theoretical and simulated results.

Theoretical transmission

The calculations of the theoretical total transmission coefficients are done by equation (2.99) in section 2.4.

Figure 4.7 shows the theoretically achieved total transmission through PI and the PI-samples coated with both 10 μm and 20 μm thick PVDF-layers. Table 4.11 lists the values of the theoretically obtained amplitude spectrum $A_1(f')$ at frequencies f' of the PI-sample, together with an estimation of the wavelength λ and the sample thickness $\widehat{d}$. Table 4.12 and 4.13 lists the theoretically obtained values of the total transmission $A_1(f')$ at the frequencies f', for the PI-sample coated with respectively 10 μm and 20 μm PVDF.

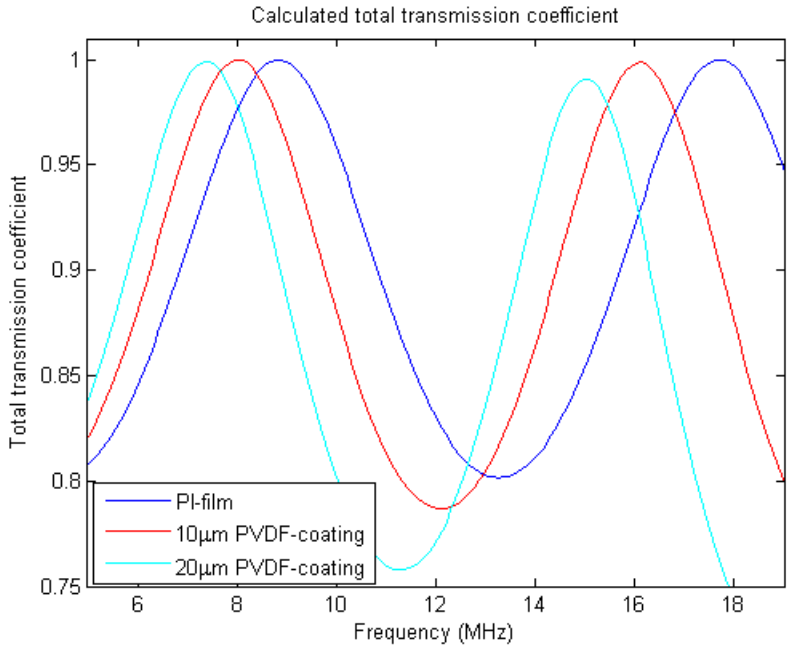

Figure 4.7: Theoretical transmission through PI and PI-samples coated with both 10 μm and 20 μm PVDF-layers.

Amplitude spectrum of PI-sample from theory

	First maximum	Minimum	Second maximum
$\mathbf{A_1(f')}$	1.00	0.80	1.00
f' [MHz]	8.88	13.25	17.72
λ **[μm]**	253	169	127
$\widehat{\mathbf{d}}$ $[\mu m]$	$\lambda/2 = 126$	$3\lambda/4 = 127$	$\lambda = 127$

Table 4.11: Transmission at resonance frequencies f' for the PI-sample in Figure 4.7. Wave length λ estimated by equation (3.11), and sample thickness $\widehat{d}$ estimated by equation (3.13).

Amplitude spectrum for PI-sample with 10 μm thick PVDF-coating from theory

	First maximum	Minimum	Second maximum
$\mathbf{A_1(f')}$	1.00	0.79	1.00
f' [MHz]	8.03	12.12	16.10

Table 4.12: Transmission at resonance frequencies for the PI-sample with 10 μm thick PVDF-coating in Figure 4.7.

Amplitude spectrum from theory for PI-sample with 20 μm thick PVDF-coating.

	First maximum	Minimum	Second maximum
$\mathbf{A_1(f')}$	1.00	0.76	0.99
f' [MHz]	7.36	11.26	15.06

Table 4.13: Transmission at resonance frequencies for the PI-sample with 20 μm thick PVDF-coating in Figure 4.7.

Simulated transmission

This section shows the results from the simulations done through the COMSOL-models described in section 3.2.1. The waveforms and frequency spectra from the simulations in the models with PI and PI coated with 10- and 20 μm thick PVDF are shown in Figure 4.8, together with the waveform and frequency spectrum obtained from the received signal simulated by the model with only water between the transducers. Table 4.14 lists the System Fidelity Factors for the waveforms in Figure 4.8a.

The amplitude spectra for the simulated signals through PI and PI with PVDF-coating thickness of both 10- and 20 μm are shown in Figure 4.9. Table 4.15 lists the values of the amplitude spectrum at frequencies f', of the obtained signal from the simulation through PI. The values of the amplitude spectra at frequencies f' of the obtained signals from the simulations through the PVDF-coated PI-samples are given by Table 4.16 and 4.17, respectively, for the 10- and 20 μm thick coating.

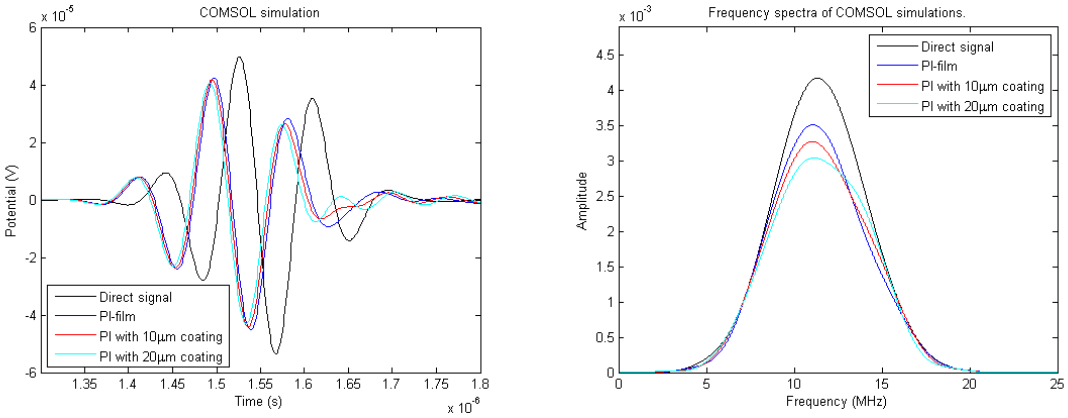

(a) Received waveform.

(b) Frequency spectra.

Figure 4.8: COMSOL-simulated received waveforms and their frequency spectra, through PI-film and PI-samples with 10- and 20 μm thick PVDF-coating.

System Fidelity Factor

Signal a	**Signal b**	**SFF with 10 μm coating**	**SFF with 20 μm coating**
PI-film	Direct signal	0.99	0.99
PI-film	PVDF-coating	0.996	0.99
PVDF-coating	Direct signal	0.99	0.99
10 μm coating	20 μm coating	0.996	

Table 4.14: System Fidelity Factor for simulated waveforms. "Signal a" is compared to "Signal b".

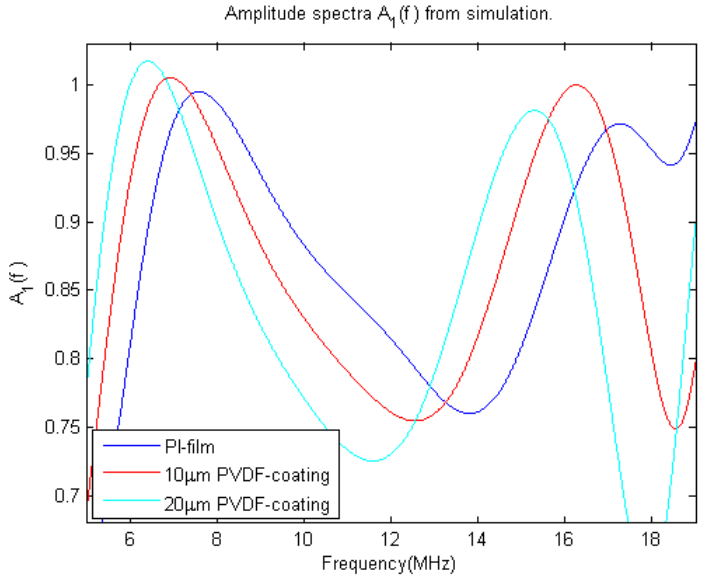

Figure 4.9: Amplitude spectra from simulation.

Simulated amplitude spectrum of PI-film

	First maximum	**Minimum**	**Second maximum**
$\mathbf{A_1(f)}$	0.99	0.76	0.97
f' [MHz]	7.60	13.82	17.28
λ **[μm]**	295	162	130
$\widehat{\mathbf{d}}$ **[μm]**	$\lambda/2 = 147$	$3\lambda/4 = 121$	$\lambda = 130$

Table 4.15: Transmission at resonance frequencies f' for the PI-film in Figure 4.9. Wave length λ estimated by equation (3.11), and sample thickness $\widehat{d}$ estimated by equation (3.13).

Simulated amplitude spectrum of PI-film with 10 μm thick PVDF-coating.

	First maximum	**Minimum**	**Second maximum**
$\mathbf{A_1(f')}$	1.00	0.75	1.00
f' [MHz]	6.95	12.57	16.28

Table 4.16: Transmission at resonance frequencies for the PI-film with 10 μm thick PVDF-coating in Figure 4.9.

Simulated amplitude spectrum of PI-film with 20 μm thick PVDF-coating.

	First maximum	Minimum	Second maximum
$\mathbf{A_1(f')}$	1.02	0.72	0.98
f' [MHz]	6.43	11.60	15.31

Table 4.17: Transmission at resonance frequencies for the PI-film with 20 μm thick PVDF-coating in Figure 4.9.

4.3 Comparison between experimental, numerical and theoretical results

This section gives a systematic comparison between the experimental, numerical and theoretically obtained results where this is possible.

As listed by Table 3.4 in section 3.1.2, Sample 1 was measured to be approximately 150 μm thick and Sample 2 was 137 μm. Therefore the amplitude spectrum of Sample 1 are plotted together with, and compared with the simulated 20 μm thick PVDF-coated PI-sample. For the same reason, the amplitude spectrum obtained through Sample 2 are compared with and plotted together with the simulated 10 μm thick PVDF-coated PI-sample.

4.3.1 Thick samples

Table 4.18 compares the damping factors β obtained for PEI, PMMA and PC through the experimental measurements with the 10 MHz- and 20 MHz transducer pairs. A comparison between the total transmission coefficients for these three polymers obtained experimentally with the two sets of transducers are given in Table 4.19.

Table 4.20 compares the theoretically obtained total transmission coefficients for PEI, PMMA and PC with those experimentally obtained with the 10 MHz transducers. The theoretical and experimentally obtained total transmission coefficients with the 20 MHz transducers are compared in Table 4.21.

Comparison between experimentally obtained damping factors β

Polymer	Experiments at 10 MHz	Experiments at 20 MHz	Deviation
PEI	0.49	0.41	16.3 %
PMMA	0.71	0.64	9.8 %
PC	4.38	4.14	5.5 %

Table 4.18: Comparison of damping factors of PEI, PMMA and PC found experimentally with the 10 MHz and the 20 MHz transducers.

Comparison between experimentally obtained total transmission coefficients

Polymer	Experiments at 10 MHz	Experiments at 20 MHz	Deviation
PEI	0.81	0.78	3.7 %
PMMA	0.77	0.76	1.3 %
PC	0.89	0.77	13.5 %

Table 4.19: Comparison of the total transmission coefficients of PEI, PMMA and PC found experimentally with the 10 MHz and the 20 MHz transducers.

Comparison between total transmission coefficients obtained theoretically and experimentally with the 10 MHz transducers

Polymer	Theoretical	Experiments at 10 MHz	Deviation
PEI	0.87	0.81	6.9 %
PMMA	0.86	0.77	10.5 %
PC	0.91	0.89	2.2 %

Table 4.20: Comparison of the total transmission coefficients of PEI, PMMA and PC found theoretically based on the impedances given in Table 3.2 and Table 3.3, and experimentally with the 10 MHz transducers.

Comparison between total transmission coefficients obtained theoretically and experimentally with the 20 MHz transducers

Polymer	Theoretical	Experiments at 20 MHz	Deviation
PEI	0.87	0.78	10.3 %
PMMA	0.86	0.76	11.6 %
PC	0.91	0.77	15.4 %

Table 4.21: Comparison of the total transmission coefficients of PEI, PMMA and PC found theoretically based on the impedances given in Table 3.2 and Table 3.3, and experimentally with the 20 MHz transducers.

4.3.2 Thin samples

Figure 4.10 shows the theoretically achieved amplitude spectrum of a PI-sample together with the spectra obtained experimentally and through simulation. The values of the amplitude spectra at frequencies f' for the PI-sample are compared in Table 4.22.

Since the left and right sides of Sample 1 and Sample 2 are very similar as seen in Figure 4.4 and 4.6, respectively, only the right sides of the samples are used in the comparison with the theoretical and numerical results.

Figure 4.11 shows the experimentally obtained amplitude spectrum of Sample 2 together with the theoretical and simulated amplitude spectra of the 10μm thick PVDF-coated PI-film. Table 4.23 compares the experimentally obtained values of the amplitude spectrum at frequencies f' for Sample 2, with values achieved theoretically and by simulation for a 10μm thick PVDF-coated PI-film.

Figure 4.12 shows the theoretical and simulated amplitude spectra of the 20μm thick PVDF-coated PI-sample together with the experimentally obtained amplitude spectrum of Sample 1. The theoretical and numerically obtained amplitude spectra at frequencies f' for a 20μm thick PVDF-coated PI-sample, are compared in Table 4.24 with the experimentally obtained values for Sample 1.

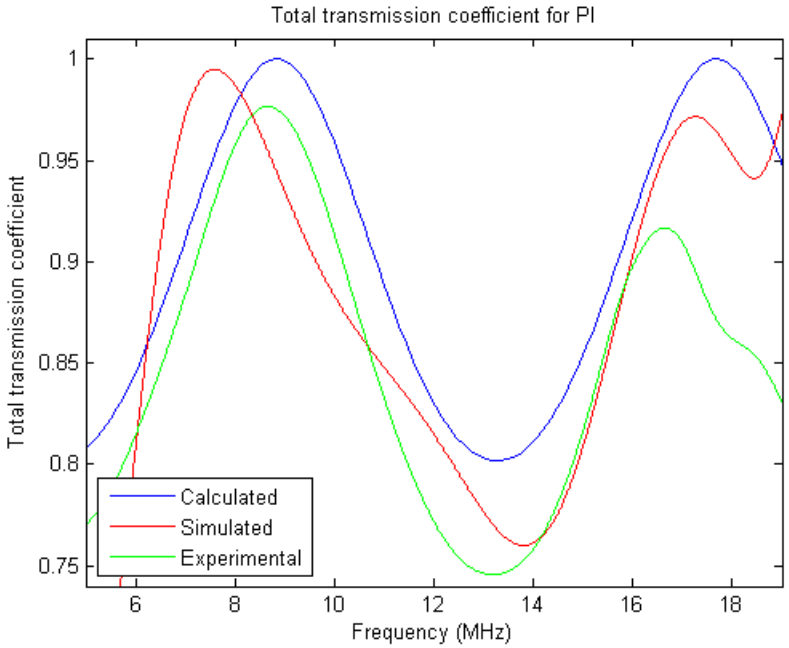

Figure 4.10: Theoretical, simulated and experimentally achieved amplitude spectra of a PI sample plotted together.

Amplitude spectra comparison of PI

	First maximum		Minimum		Second maximum	
	$A_1(f')$	f' [MHz]	$A_1(f')$	f' [MHz]	$A_1(f')$	f' [MHz]
Theoretical	1.00	8.88	0.80	13.25	1.00	17.72
Numerical	0.99	7.60	0.76	13.82	0.97	17.28
Experimental	0.98	8.67	0.74	13.20	0.92	16.65
Maximum deviation	2.0 %	14.4 %	7.5 %	4.5 %	8.0 %	6.0 %

Table 4.22: Comparison between the amplitude spectra obtained theoretically, numerically and experimentally for PI.

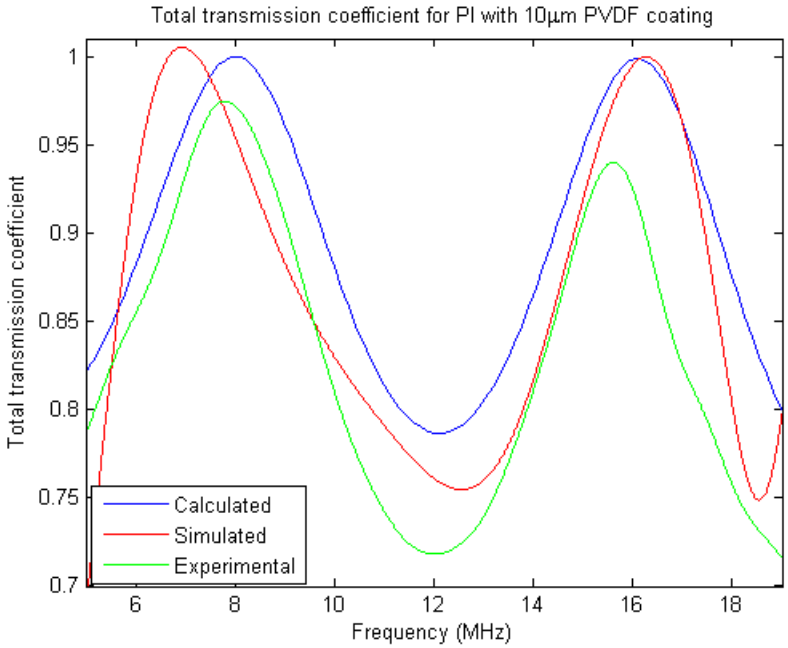

Figure 4.11: Calculated and simulated amplitude spectra of a 10 μm thick PVDF-coated PI sample plotted together with the experimentally obtained amplitude spectrum of the right side of Sample 2.

Amplitude spectra comparison of PI-samples with 10 μm thick PVDF-coating

	First maximum		**Minimum**		**Second maximum**	
	A_1(f')	**f' [MHz]**	**A_1(f')**	**f' [MHz]**	**A_1(f')**	**f' [MHz]**
Theoretical	1.00	8.03	0.79	12.12	1.00	16.10
Numerical	1.00	6.95	0.75	12.57	1.00	16.28
Experimental	0.97	7.81	0.72	12.02	0.94	15.61
Maximum deviation	3.0 %	13.4 %	8.9 %	4.4 %	6.0 %	4.1 %

Table 4.23: Comparison between the amplitude spectra obtained theoretically, numerically and experimentally between PI-samples with 10 μm thick PVDF-coating and the right side of sample 2.

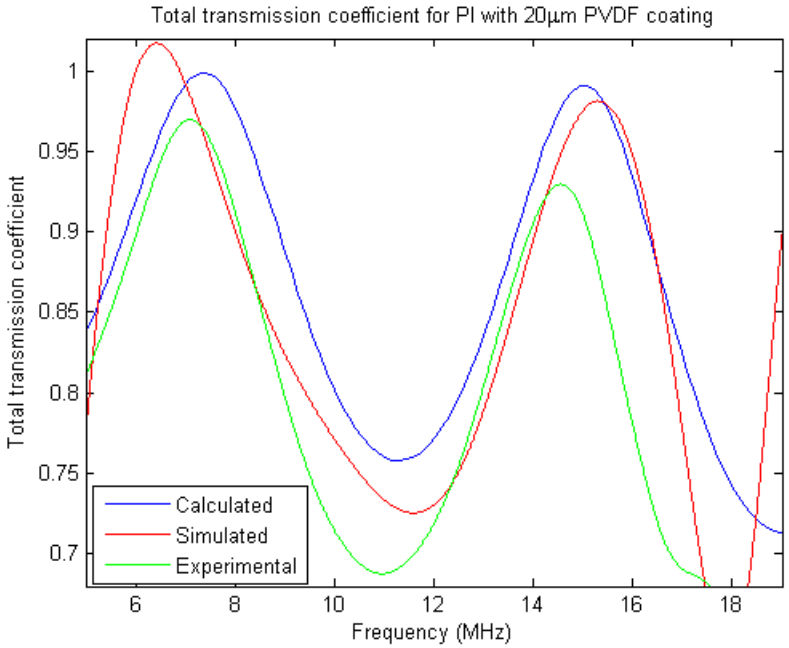

Figure 4.12: Calculated and simulated amplitude spectra of a 20 μm thick PVDF-coated PI sample plotted together with the experimentally achieved amplitude spectrum of the right side of Sample 1.

Amplitude spectra comparison of PI-samples with 20 μm thick PVDF-coating

	First maximum		Minimum		Second maximum	
	$A_1(f')$	f' [MHz]	$A_1(f')$	f' [MHz]	$A_1(f')$	f' [MHz]
Theoretical	1.00	7.36	0.76	11.26	0.99	15.06
Numerical	1.02	6.43	0.72	11.60	0.98	15.31
Experimental	0.97	7.10	0.69	10.97	0.93	14.56
Maximum deviation	4.9 %	12.6 %	9.2 %	5.4 %	6.1 %	4.9 %

Table 4.24: Comparison between the amplitude spectra obtained theoretically, numerically and experimentally between PI-samples with 20 μm thick PVDF-coating and the right side of Sample 1.

Chapter 5

Discussion

5.1 Thick samples

Measurements were done with both 10 MHz- and 20 MHz transducers through the thick material samples PEI, PMMA and PC. As expected for the measurements done with both sets of transducers, the amplitude spectra decreased linearly as the frequency increased, inside a frequency interval Δf around the applied center frequency.

For the 10 MHz transducers, this interval was chosen between 5- and 15 MHz for the PEI and PMMA samples, and between 5- and 14 MHz for the polycarbonate. For the 20 MHz transducers, all frequency intervals were between 9- and 25 MHz. Outside of these intervals the information in the signals was low, and the effects from the noise floor got visible. The linearity of the dataset was therefore lost.

The deviation of the damping factors found with both pairs of transducers are given in Table 4.18 in percents. PEI had the highest deviation in damping factors of 16.3 %.

The article "Experimental study of the acoustical properties of polymers utilized to construct PVDF ultrasonic transducers and the acousto-electric properties of PVDF and P(VDF/TrFE) films" [4] presents a damping factor β for PMMA of 1.4 dB/cm MHz. In this thesis, the damping factor for PMMA found with the 10 MHz transducers was 0.71 dB/cm MHz, that is around 51% of the damping factor from the article. The damping factor found with the 20 MHz transducers were 0.64 dB/cm MHz, which is approximately 46% of that given for PMMA by the article.

The deviation in percents for the total transmission coefficients found with the two pairs of transducers are given in Table 4.19. The measured total transmission coefficients of PEI and PMMA have a respective difference of 3.7 % and 1.3 %. The deviation in the results of PC were 13.5 %. The obtained total transmission coefficients of both PEI and PMMA are therefore considered to coincidence well. The result for PC however does not correspond to the same degree. This could be a result of the LS-line being very steep compared to the two other as seen in Figure 4.2, which made it harder to define an appropriate frequency interval.

The theoretical transmission coefficients in Table 4.10 in section 4.2, was obtained by applying the the impedances given for the polymers and water by Table 3.2 and 3.3 in section 3.1.2, to equation (2.65) in section 2.3.2. During the production of a polymer there are many factors that could create variations in the acoustic properties. Some polymers, like PMMA, also have numerous subtypes with different properties [7] [4]. Therefore, since the impedances applied in the calculation are based on material properties found from different books and articles, the theoretical values for the total transmission were expected to differ from the experimentally obtained values.

From Table 4.20, we can see that the theoretical total transmission coefficient for PC agrees with the experimentally obtained value around 10 MHz, with a deviation of only 2.2 %. Table 4.21 shows that the theoretical total transmission coefficient for PC deviates from the experimentally obtained value at 20 MHz by 15.4 %. Because of this, we can assume that the value for PC obtained by the 10 MHz transducers are the most reliable. Overall, the results from the 10 MHz transducers deviates less from the theoretical values than those from the 20 MHz transducers.

5.2 Thin samples

Measurements were done only with the pair of 10 MHz transducers for the PI-film, for Sample 1 and Sample 2. Theoretic and numerical investigation of these samples were also performed.

As described earlier, Sample 1 and Sample 2 were PI-films coated with PVDF of two different thicknesses. The uncoated PI-film and the films used underneath the coating in Sample 1 and 2 were assumed to have the same thickness since they came from the same shipment. From production specification the thickness of the PI was claimed to be 127 μm. However, measurements of the film used as a sample suggested that the thickness was varying around 130 μm by $\pm$ 2 μm. Taking the uncertainties into account, we might from the thickness measurements of Sample 1 and 2 given by Table 3.4 assume that the coating of Sample 1 was approximately 20 μm thick and that the coating of Sample 2 was about 10 μm.

5.2.1 Coating on treated and untreated PI-surfaces

Two equally created PVDF-coated PI-films were used to investigate the transmission effects of surface treatment between layers. Half the surface of both samples were treated before the coating was spun on, while the other half was left untreated. This ensured less uncertainties regarding the divination in coating thickness between the treated and untreated sides of the sample.

In Figure 4.3 the waveforms and frequency spectra of the received signals through both the left and right side of Sample 1 are plotted together. The same is done in Figure 4.5 for Sample 2. In both cases, there are no visible differences between neither the waveforms nor the frequency spectra obtained through the left and right sides of the samples. Table 4.4 shows that the estimated System Fidelity Factor between the left and right sides of Sample 1 is equal to 1. The same results yields for the estimated System Fidelity Factor between the treated and untreated side for Sample 2, as given in Table 4.7. This means that the received waveforms through both the treated and the untreated side of the samples had the exact same shape.

Thus, treating the surface of the PI-film before spinning the coating on it, did not have any effects on the transmission properties that could be detected with the applied frequency.

5.2.2 Amplitude spectrum

As expected from the theory, inside a frequency interval around the applied center frequency, the amplitude spectrum of the received signals from both the experiments and the simulations had a periodic dependence on the frequency. In the results, the amplitude spectra were presented in the interval where this behavior was found.

The same material parameters for water and the polymers were used for both the theoretical and simulated methods. To match the claimed thickness of the physical PI-film from the experiments, the thickness of the PI were for both methods defined as exactly 127 μm.

The theoretical amplitude spectrum was based on a 1-D model without damping in the material(s), and perfect transmission at the resonant frequencies was expected. The simulations in COMSOL were done in 2-D models, because of diffraction the transmission at the resonant frequencies were not anticipated to be perfect. The same yields for the experiments where there in addition were sources of errors as discussed in section 5.3. The maximum transmission was therefore expected to be highest for the theoretical amplitude spectra, lower for the 2-D simulation and even lower for the results from the experiments.

The highest deviation between the experimental, numerical and theoretical resonant frequencies are for all three samples and models the ones found at the first amplitude maxima. In all three cases the model causing the high deviation was the numerical. This could be an effect originating from the backing layer, where the signal may not have been damped enough. At the second maxima however, the resonant frequencies for the theoretical and numerical models are closer than that of the experimental.

The frequencies f' at the maximums and minimum of the amplitude spectra are highest for the measurements through only PI-film. The frequencies f' decreases when the PVDF-coating of 10 μm is added, and becomes even lower for the PI coated with 20 μm of PVDF. This trend is reflected in all three methods, and can be observed in Figure 4.7 for the theoretical case and in Figure 4.9 for the simulated method.

Since there were no differences between the left and right sides of Sample 1 and Sample 2 found with the frequency used in this thesis, only the right sides of the samples were chosen to represent Sample 1 and Sample 2 when comparing their amplitude spectra with the theoretical and numerical solutions.

PI-sample

In Figure 4.10 the theoretical, simulated and experimentally obtained amplitude spectra for PI are plotted together. The total transmission at the two maximums and at the minimum are listed in Table 4.22 for all three methods, and compared by stating the maximum deviation between them. The table also compares the maximum deviation of the frequency f' at the maximums and minimums between the methods. From this we see that the amplitude spectra obtained through experiments, simulations and from theory do correspond to some degree.

To estimate the thickness of the PI-sample from the amplitude spectra obtained by all three methods, equation (3.13) in section 3.3.2 and the theoretical sound velocity of 2256 m/s listed by Table 3.5 in section 3.2.1, were applied on the resonant frequencies. The estimated thicknesses $\widehat{d}$ for the PI-film used in the experiments are given in Table 4.3, and seems to agree very well with the thickness measured with a micrometer.

The speed of sound in the physical PI-film was unknown. The estimation $\widehat{c}_{PI} = 2254$ m/s is presented in Table 4.3, which is found by using the measured thickness d, and the first resonant frequency f' from the experiment in equation (3.14) in section 3.3.2. This estimation is very good compared the theoretical sound velocity of 2256 m/s, used in the estimation of wavelength and thickness $\widehat{d}$ as mentioned above.

PI with PVDF-coating

The amplitude spectra of the PI coated with 10μm PVDF obtained from theory and through simulation are plotted together with the experimentally obtained amplitude spectra of Sample 2 in Figure 4.11. As for the case with PI discussed above, the values of the transmission at resonant frequencies for the three methods are listed in Table 4.23, and compared by showing the maximum deviation in percents.

The amplitude spectra for PI with 20 μm PVDF-coating found through theory and simulations, are shown together with the experimentally obtained amplitude spectrum of Sample 1 in Figure 4.12. Table 4.24 presents a comparison between the theoretical, numerical and experimentally obtained transmission at the resonant frequencies.

Because of the differences between the three models, the deviations between them are considered to be low in both cases.

Estimations of thickness were not made for Sample 1 and Sample 2. This was because the sound velocity through the samples were unknown, since they consisted of two different polymers.

5.3 Uncertainty analysis

There are several sources of error to take into account when analyzing the data from the experiments. Comparing experimental results to numerical results produces points of uncertainties regarding their differences.

The following uncertainties are listed from the assumed worst to the mildest.

Experimental versus numerical: Although the COMSOL models were implemented to match the experimental setup, some differences must be expected. The pulse $U_n(t)$ applied in the numerical model were programmed to have the same shape as $U_e(t)$ from the experiments. However, $U_e(t)$ was sent through several wires, a signal generator and finally a physical transducer before it was transmitted. The shape of the experimentally transmitted pulse U(t) is therefore assumed to have changed somewhat. This means that $U_n(t)$ and U(t) is likely to have different shapes.

Frequency interval: The definition of the frequency interval Δf in which the first order least squares method was based to calculate the amplitude spectra of the thick samples, was seen to influence the total transmission coefficients as described in section 3.3.1. A $\pm$ 1 MHz change in the interval was seen to result in around $\pm$ 1.5 % difference in the total transmission coefficient.

Thickness variation: The PI-film used in the experiments had a thickness variation of $\pm 3\ \mu m$. The PVDF-coating on the PI was manually spun on top, thus small variations in the thickness of the coating are expected.

Sample 1 and Sample 2 were compared to the numerical and theoretical models with 20- and 10 μm coating thicknesses, respectively. The differences in both the thickness of the PI and in the coating, between the experimental and numerical models must be considered in the comparison.

Clouded water: Tap water was used in the experiments. When newly tapped water was used in the tank, many small air bubbles would appear on the surfaces of all the equipment. Such air bubbles are a result of how the properties of water changes with temperature and pressure. Cold water can hold more air than hot water, and water under pressure in the tab has the ability to hold more air than water under less pressure such as in a tank [29].

Tiny air bubbles would appear on the sensors, which could distort and damp the signal. To remove the bubbles from the sensors, a finger was used. This could leave a fingerprint which again could cause distortion of the signal. Systematic attempts to remove of such bubbles were made throughout the experiments.

Positioning of the sample: For each new measurement with the thin samples, the samples were attached to the frame manually. Since they were only 130- 150 μm thick, their shapes after being fastened to the frame could vary. The frame had to be detached from the framework for each new sample. The coated samples had to be attached twice, in order to do the measurements through both the left and right sides.

The frame itself was attached manually to the slider on the framework. The position of the frame on the slider was initially chosen by moving them close to a transducer and then position the frame by eye on the slider, such that the transducer pointed to the center of the frame hole. Then a little mark was made on the slider to later be able to position the frame on the same spot.

Shear waves:[22] [7] If a thick sample, or the frame with one of the thin samples attached to it was not perpendicular to the signal coming from the transducer, shear waves could form in the polymer. There was variations in the smoothness of the surfaces of the thick samples; as seen in Figure 3.4 of the samples applied, the surface of PEI was quite coarse. Shear waves could also be formed as a result of the thin samples not sitting straight in the frame.

Measurements: The measurements for the PI-film and Sample 1 were done the same day in a clean tank with fresh water. Measurements for Sample 2 were done earlier, and in two days old temperature regulated water. Both the uncertainties of dirty and clouded water might have an effect on the differences this produces, as the fresh water was clean but cloudy and the old water

was not clouded but might have been a little dirty.

Focus: The 10 MHz transducers had a target focus in water at about 5.3 cm. The focus length of the 20 MHz transducers through water was at around 5.1 cm. The distance between the sending and receiving transducer was chosen manually with a ruler to be 10 cm, and kept at the same positions throughout the experiments. The placement of each of the samples with respect to the transducers, was decided by viewing the first reflection received with both transducers on the oscilloscope. The sample could then be moved such that the echoes were positioned at the same place. With this method the middle of the inserted sample would be in the center of the transducer system. Therefore, the samples might be slightly outside of focus.

Dirty water: Since the tank were open, and since some of the equipment had to be taken out of the water to change samples, different types of filth such as hair would gather up in the tank. When water is left still in a tank for a long time, bacterias and algae will form on the walls of the tank. When fresh water is pored in to adjust temperature, or when equipment is submerged, some of this will be knocked off the walls and start to float around. Any type of such objects in the water could cause distortions of the signal.

Water temperature: The transducers applied in these experiments were manufactured to operate best at a temperature around 20 °C. The room in which all the experiments were made, had an average temperature of 15 °C, so the water temperature was always decreasing. For theoretical calculations the temperature was always assumed to be around 20 °C.

The temperature of the water while doing the measurements for the thick samples was 25.5 °C in the beginning and fell towards 21.3 °C in the end. Changes of this size in the temperature has an impact on the impedance in water [7].

For the experiments done with the thin samples, the temperature of the water bath was chosen and regulated to stay around 20.5 °C.

Attenuation in water: Since the samples had different thicknesses, there was a variation in distance that the signal would travel through water. The attenuation in the water would therefore change slightly from sample to sample. Table 3.3 gives an attenuation factor β in water at 20 °C of 0.002 dB/cm MHz.

Chapter 6

Conclusion and further work

The experimental results for total transmission coefficients through the thick samples coincided to some degree with the values found by using common impedances in equation (2.65) in section 2.3.2 in the theory of single interface transmission. Comparison between the total transmission coefficients obtained by theory and through the experiments for both sets of transducers, indicates that the results obtained with the 10 MHz transducers given in Table 4.1, were the most reliable.

The amplitude spectra found through experiments for the thin samples did to some extent coincide with both the theory and the numerical results. Based on the resonant frequencies f' from the amplitude spectrum obtained through experiments, good estimations of the thickness of- and the sound speed through the PI-film was found. As expected, the maximum transmission at resonant frequencies were perfect for the theoretical model. For the 10 μm coated PI-film the numerically obtained maximum transmission was also perfect. For the two other numerical models the maximum transmission were almost perfect. Finally, also as expected, the experimentally obtained amplitude spectra gave the lowest maximum transmission.

Their differences taken to account, the theoretical, numerical and experimental results were found to correspond. This means that the equation for total transmission given by equation (2.99) in section 2.4 is a good estimation for the samples applied. The numerical models that were implemented in COMSOL specifically to match the experiments, also provided quite good estimations.

In the future it could be interesting to see how changing the damping factor in the backing layer would effect the reliability of the COMSOL models.

Experimental investigation of two PI-films coated with PVDF in two different thicknesses were

performed with a center frequency of 10 MHz. Half of the PI-surfaces were in both cases treated before the coating was spun on. No effects on transmission properties were found when comparing the treated surfaces of the two samples with the untreated surfaces.

Further work regarding how the transmission properties of a two-layer sample are affected by treating the surface between the layers, may involve doing this experiment at higher frequencies such that the wavelength becomes small compared to the coating.

List of Figures

List of Tables

Bibliography

[1] Michael Ainslie. *Principles of Sonar Performance Modelling.* Berlin, Heidelberg : Springer-Verlag Berlin Heidelberg, 2010.

[2] Helge Øberg. Ultrasound sensor for biomedical applications. Master's thesis, University of Tromsø, 2011.

[3] David T. Blackstock. *Fundamentals of physical acoustics.* John Wiley & Sons, Inc., 2000.

[4] P.E. Bloomfield, Wei-Jung Lo, and P.A. Lewin. Experimental study of the acoustical properties of polymers utilized to construct pvdf ultrasonic transducers and the acousto-electric properties of pvdf and p(vdf/trfe) films. *Ultrasonics, Ferroelectrics and Frequency Control, IEEE Transactions on*, 47(6):1397–1405, 2000.

[5] Jonny Österman Carl Nordling. *Physics Handbook for Science and Engineering.* Studentlitteratur, 2006.

[6] J.E. Carlson, J. Van Deventer, A. Scolan, and C. Carlander. Frequency and temperature dependence of acoustic properties of polymers used in pulse-echo systems. In *Ultrasonics, 2003 IEEE Symposium on*, volume 1, pages 885–888 Vol.1, 2003.

[7] J. David N. Cheeke. *Fundamentals and Applications of ultrasonic waves.* CRC Press LLC, 2002.

[8] Susan Jane Colley. *Vector Calculus.* Pearson Education, Inc., 2006.

[9] COMSOL. http://www.comsol.com/products/multiphysics/.

[10] R. Djakaria, B.I. Chandran, M. H. Gordon, W.F. Schmidt, and T.G. Lenihan. Determination of young's modulus of thin films used in embedded passive devices. In *Electronic Components and Technology Conference, 1997. Proceedings., 47th*, pages 745–749, 1997.

[11] Trude Ediassen Grimstad. Ultrasonic diffraction fields in fluids and elastic materials. Project paper in Electrical Engineering.

[12] W. Hackmann. *Seek and Strike: Sonar, Anti-submarine Warfare and the Royal Navy 1914-54*. HM Stationery Office, London, 1984.

[13] John F. Hall. Problems encountered from use (or misuse) of rayleigh damping. *Earthquake engeneering and structuran dynamics*, 35:525–545, 2005.

[14] P. He. Experimental verification of models for determining dispersion from attenuation. *Ultrasonics, Ferroelectrics and Frequency Control, IEEE Transactions on*, 46(3):706–714, 1999.

[15] Chris Rorres Howard Anton. *Elementary Linear Algebra*. Anton Textbooks, Inc, 2005.

[16] Ronald W. Schafer James H. McClellan and Mark A. Yoder. *Signal Processing First*. Pearson Education, Inc., 2003.

[17] Gunnar Løvhøiden Jan R. Lien. *Generell fysikk for universiteter og høgskoler, bind 1 Mekanikk*. Universitetsforlaget, 2004.

[18] C.C. Lee, M. Lahham, and B. G. Martin. Experimental verification of the kramers-kronig relationship for acoustic waves. *Ultrasonics, Ferroelectrics and Frequency Control, IEEE Transactions on*, 37(4):286–294, 1990.

[19] K mac Plastics. http://k-mac-plastics.net/data

[20] Frank Melandsø. Lecture notes. 2012.

[21] NDTnet. http://www.ndt.net/links/proper.htm.

[22] Morten Wollert Nygren. Finite element modeling of piezoelectric ultrasonic transducers. Master's thesis, Norwegian University of Science and Technology, 2011.

[23] University of Alberta. http://www.100years.ualberta.ca/achievements.cfm?profile=11.

[24] G. Quintero, J.-F. Zürcher, and A.K. Skrivervik. System fidelity factor: A new method for comparing uwb antennas. *Antennas and Propagation, IEEE Transactions on*, 59(7):2502–2512, 2011.

[25] Daniel R. Raichel. *The Science and Applications of Acoustics*. Springer Science+Business Media, LLC, 2006.

[26] Karl Rottman. *Matematisk formelsamling*. Spektrum forlag, 2008.

[27] Daniel Royer and Eugène Dieulesaint. *Elastic Waves in Solids I. Free and Guided Proagation.* Springer-Verlag Berlin Heidelberg, 2000.

[28] Mauricio D Sacchi Dean Ta Rui Zheng, Lawrence H Le and Edmond Lou. Spectral ratio method to estimate broadband ultrasound attenuation of cortical bones in vitro using multiple reflections. *IOP publishing Ltd. Physics in Medicine and Biology*, 52:5855–5869, 2007.

[29] U.S. Geological Survey. http://ga.water.usgs.gov/edu/qa-chemical-cloudy.html.

[30] Thomas L. Szabo. *Diagnostic Ultrasound Imaging: Inside out.* Elsevier Inc., 2004.

[31] M. Vazquez, L. Leija, A. Vera, A. Ramos, and E. Moreno. Experimental estimation of acoustic attenuation and dispersion. In *Electrical and Electronics Engineering, 2005 2nd International Conference on*, pages 156–159, 2005.